



# Impact of Surfactants on the Performance of Clopidogrel-Copovidone Amorphous Solid Dispersions: Increased Drug Loading and Stabilization of Nanodroplets

Clara E. Correa Soto<sup>1</sup> · Yi Gao<sup>2</sup> · Anura S. Indulkar<sup>3</sup> · Keisuke Ueda<sup>4</sup> · Geoff G. Z. Zhang<sup>3</sup> · Lynne S. Taylor<sup>1</sup>

Received: 20 October 2021 / Accepted: 17 December 2021 / Published online: 10 January 2022

© The Author(s), under exclusive licence to Springer Science+Business Media, LLC, part of Springer Nature 2022

## ABSTRACT

**Purpose** Surfactants are increasingly being added to amorphous solid dispersion (ASDs) formulations to enhance processability and release performance. The goal of the current work was to investigate the impact of cationic, anionic and non-ionic surfactants on the rate and extent of clopidogrel (CPD) release from copovidone-based ASDs.

**Methods** CPD release was evaluated for ASDs with different drug loadings using a surface normalized intrinsic dissolution apparatus. Studies were also carried out using dynamic light scattering, zeta potential

measurements, and nuclear magnetic resonance spectroscopy to probe the impact of surfactants on drug-rich nanodroplet physical stability and clopidogrel-surfactant interactions.

**Results** CPD ASDs showed good release for drug loadings as high as 40%, before the release fell off a cliff at higher drug loadings. Only sodium dodecyl sulfate, added at a 5% level, was able to improve the release at 50% drug loading, with other surfactants proving to be ineffective. However, some of the surfactants evaluated did show some benefits in improving nanodroplet stability against size enlargement. Ionic and non-ionic surfactants were observed to interact differently with CPD-rich nanodroplets, and variations in the kinetics and morphology of water-induced phase separation were noted in the presence and absence of surfactants in ASD films.

**Conclusions** In summary, addition of surfactants to ASD formulations may lead to some improvements in formulation performance, but predictive capabilities and mechanisms of surfactant effect still require further studies.

**Supplementary Information** The online version contains supplementary material available at <https://doi.org/10.1007/s11095-021-03159-w>.

✉ Geoff G. Z. Zhang  
Geoff.GZ.Zhang@abbvie.com

✉ Lynne S. Taylor  
lstaylor@purdue.edu

<sup>1</sup> Department of Industrial and Physical Pharmacy  
College of Pharmacy, Purdue University,  
Indiana 47907 West Lafayette, USA

<sup>2</sup> Science and Technology, Operations, AbbVie Inc.,  
North Chicago, Illinois 60064, USA

<sup>3</sup> Drug Product Development, Research  
and Development, AbbVie Inc., North Chicago,  
Illinois 60064, USA

<sup>4</sup> Graduate School of Pharmaceutical Sciences, Chiba  
University, 1-8-1 Inohana, Chuo-ku, Chiba 260-8675,  
Japan

**KEY WORDS** amorphous solid dispersion ·  
nanodroplets · release · surfactants

## ABBREVIATIONS

API	Active pharmaceutical ingredient
ASD	Amorphous solid dispersion
AUC	Area under the curve
CMC	Critical micelle concentration
CPD	Clopidogrel
CTAB	Cetrimonium bromide
DLS	Dynamic light scattering
GLPS	Glass liquid phase separation

HLB	Hydrophilic lipophilic balance
HPLC	High performance liquid chromatography
LLPS	Liquid liquid phase separation
LoC	Limit of Congruency
NMR	Nuclear magnetic resonance
NTA	Nanoparticle tracking analysis
PVPVA	Copovidone
SDS	Sodium dodecyl sulfate
$T_g$	Glass transition temperature
TPGS	D- $\alpha$ -tocopherol polyethylene glycol 1000 succinate
TWN	Tween 80
UV	Ultraviolet

## INTRODUCTION

Solubility and permeability directly impact oral absorption, and consequently bioavailability, as outlined in the biopharmaceutical classification system (1). For solubility-limited active pharmaceutical ingredients (APIs) (class II and IV, which have high and low permeability respectively), an increase in solution concentration beyond the crystalline solubility may increase bioavailability since the absorption rate depends on the dissolved free drug concentration (2). For these classes of APIs, one of the strategies to increase transport of drugs across the membrane is to utilize an enabling formulation that leads to supersaturation. In supersaturated solutions, the equilibrium solubility is exceeded, and the solute has a higher thermodynamic activity than in a solution at equilibrium, resulting in a higher flux across a membrane. If permeability is not the rate limiting step, a higher bioavailability can be achieved (2–4).

Supersaturation results from dissolution of a higher energy solid state such as the amorphous form of an API, or from a rapid change of environment from highly soluble to less soluble conditions, for example by pH variation (5). Additionally, when the maximum supersaturation is exceeded, i.e. above the amorphous solubility, formation of drug-rich amorphous nanodroplets occurs (in the absence of crystallization) (5).

Formation of drug-rich nanodroplets, also called promiscuous aggregation, of poorly soluble drugs has been reported during high-throughput screening (HTS) assays during dilution of a concentrated drug stock solution, as well as during dissolution of drugs formulated as a high energy state (6). Nanodroplets form via liquid-liquid phase separation (LLPS) when a critical concentration is exceeded. This concentration has to exceed the binodal composition on the miscibility phase diagram for nucleated phase separation, or the spinodal composition for spontaneous phase

separation; these concentrations are typically close together for poorly soluble drugs in water (7). Above the LLPS concentration, demixing of the drug from the bulk aqueous phase occurs, leading to two liquid phases, a solvent-rich phase and a drug-rich phase (8). If the glass transition temperature ( $T_g$ ) of the drug is above the experimental temperature, then the drug-rich phase will be in the glassy state and the process can be termed glass-liquid phase separation (GLPS) (9). The LLPS concentration shows good correspondence with the amorphous solubility (binodal composition), and any additional drug added to the solution phase above the LLPS or GLPS concentration forms drug-rich nanodroplets (6, 7). The typical initial size range of the nanodroplets is 50–1000 nm (10–13). Drug-rich nanodroplets can be formed by different methods including solvent shift, amorphous solid dispersion (ASD) dissolution, and pH or solvent shift. In solvent shift, the drug is solubilized in an organic solvent, then added into an aqueous solvent; this method is extensively used during HTS (6, 14), and to determine the amorphous solubility (4, 7, 10, 15). During ASD dissolution, especially when a hydrophilic polymer drives the dissolution, the matrix components are released rapidly with the generation of API-rich nanodroplets indicating that the LLPS concentration was exceeded (2, 16). pH shift is relevant *in vivo* in particular for weak bases. During gastrointestinal transit, weakly basic drugs can undergo a decrease in solubility on transit from the low pH in the stomach where they exist in ionized form to the higher pH in the small intestine where the un-ionized form predominates (5, 10, 17, 18).

Formation of drug-rich nanodroplets during dissolution of drug formulations, especially from amorphous solid dispersions, is thought to be beneficial for bioavailability (3, 11, 19–21). First, nanodroplets may act as a reservoir; the fast dissolution of nanodroplets sustains rapid absorption by maintaining the maximum supersaturation (3). Second, the nanodroplets generated may provide benefits during absorption by drifting into the mucous layer (11, 21, 22). Wilson et al., reported an increase of the area under the curve (AUC) in a rat study following oral dosing of an enzalutamide-copovidone (PVPVA) ASD which formed nanodroplets relative to an ASD formulation that formed a supersaturated solution without nanodroplets (19). Moreover, Kesiosoglou et al., suggested that the formation of nanodroplets of 100 nm or smaller following ASD dissolution gave improved bioavailability compared to nanodroplets 200 nm or larger for anacetrapib systems (11). Similarly, Stewart et al., noted that an ASD of itraconazole with hydroxypropylmethylcellulose acetate succinate (HPMCAS) that generated drug-rich species of 150–400 nm

during dissolution showed 10–50% higher bioavailability than formulations without drug-rich nanodroplets. Additionally, in formulations where nanodroplet size increased, there was a decrease in apparent concentration in the receiver cell during flux studies (21). This suggests that formation of nanodroplets by ASD dissolution and maintenance of a small size within the available gastrointestinal (GI) transit time is important. The available transit time refers to the time the drug spends in the GI tract before reaching its absorptive site as well as its residence time at the site of absorption (18).

A supersaturated solution containing a drug-rich phase is thermodynamically metastable, consequently both drug crystallization and coarsening of the drug-rich phase may occur (23–25). The nanodroplets are dispersed in the continuous aqueous-rich phase, and can undergo coarsening by several mechanisms such as creaming, Ostwald ripening, flocculation, and coalescence (26, 27). Coarsening of the drug-rich phase may negate the reservoir effect as well as possible drifting into the mucous layer. Moreover, drug crystallization will reduce any bioavailability advantage by eliminating supersaturation.

Surfactants are widely known to stabilize a variety of dispersed systems such as emulsions and suspensions (28). Thus, they can reasonably be expected to stabilize the drug-rich nanodroplets formed upon ASD dissolution. Surfactants are commonly used in amorphous drug formulations for a variety of reasons; they have been added to improve dissolution behavior

and incorporated to aid processes such as hot melt extrusion (29–31). In solution, micellar surfactant can increase solubility, but it may decrease the drug absorption by lowering the chemical potential of the drug (4, 15, 32). Surfactant selection is largely empirical and the drug-to-surfactant ratio used typically ranges from 20:1 to 2:1 for physically stable nanocrystalline formulations and 30 to 60% w/w of the formulation for self-emulsifying formulations (33–35). The correct ratio is important since too little surfactant will allow coalescence/agglomeration while too much will promote Ostwald ripening (33). Surfactants have been also reported to induce drug crystallization in both the solid matrix and from supersaturated solutions (29, 36, 37). Thus, careful evaluation of advantages (nanodroplet size stabilization) and disadvantages (e.g. enhanced crystallization) is needed when adding surfactants to ASD formulations.

The purpose of the current study was first to evaluate the minimum concentration of surfactant required to prevent drug-rich nanodroplet size increase for at least 4 h, which is considered the biologically relevant timeframe for gastric and small intestinal transit. Second, the impact of surfactant on drug release from copovidone (PVPVA) based ASDs was evaluated.  $^1\text{H}$  nuclear magnetic resonance ( $^1\text{H}$  NMR) spectroscopy was employed to probe the mechanisms of nanodroplet size stabilization by an anionic (sodium dodecyl sulfate, SDS), a cationic (cetyltrimethylammonium bromide, CTAB), and two nonionic surfactants [*D*- $\alpha$ -tocopherol

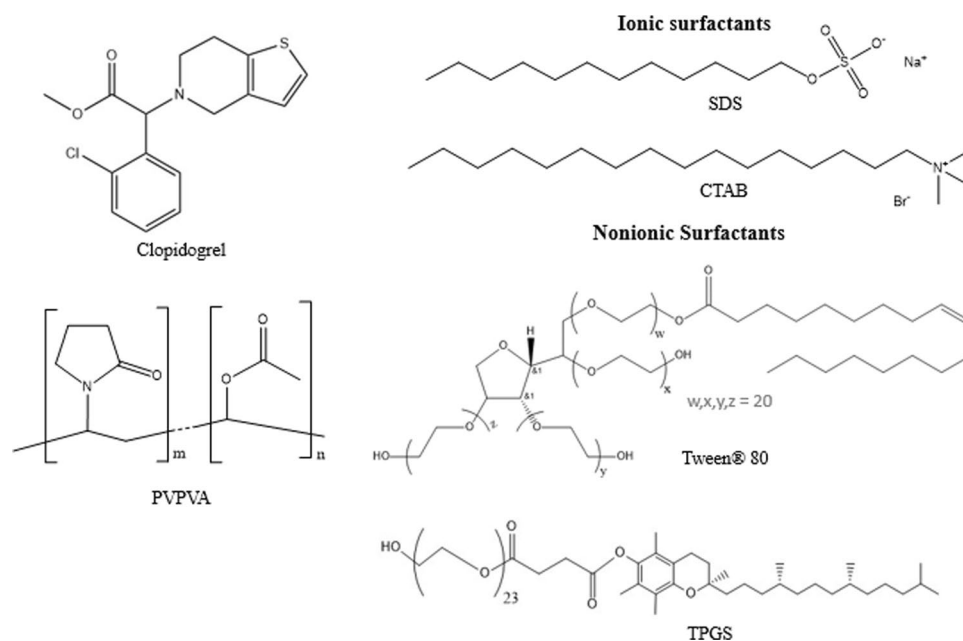


**Fig. 1** Molecular structures of clopidogrel, PVPVA, SDS, CTAB, Tween®80, and TPGS.

polyethylene glycol 1000 succinate (TPGS) and polysorbate 80]. Structures of the model compounds are shown in Fig. 1. Clopidogrel free base was selected as a model slowly-crystallizing poorly-soluble compound. An absence of crystallization over long experimental time frames enables evaluation of nanodroplet properties.

## EXPERIMENTAL SECTION

### Materials

Clopidogrel free base (CPD) was purchased from Attix Corporation (Toronto, ON). Polyvinylpyrrolidone–vinyl acetate copolymer VA64 (PVPVA) was obtained from BASF (Ludwigshafen, Germany). Sodium dodecyl sulfate (SDS), D- $\alpha$ -tocopherol polyethylene glycol 1000 succinate (TPGS) and polysorbate 80 (TWN), were purchased from Sigma Aldrich (St. Louis, MO). The supplier for cetyltrimethylammonium bromide (CTAB) was Alfa Aesar (Haverhill, MA). Deuterium oxide ( $D_2O$ ) 99.9% and deuterated methanol (methanol- $d_4$ ) were obtained from Cambridge Isotope Laboratories Inc. (Andover, MA). Sodium phosphate monobasic monohydrate and sodium phosphate dibasic anhydrous were purchased from Fisher scientific (Hampton, NH).

Experiments were conducted in phosphate buffer 50 mM pH 6.8 prepared by dissolving 3.52 g of sodium phosphate monobasic monohydrate and 3.479 g of sodium phosphate dibasic anhydrous in water to a final volume of 1000 ml where the final pH was adjusted to 6.8 with either NaOH or phosphoric acid and verified using a pH meter.

### Methods

#### *Liquid-Liquid Phase Separation (LLPS) Concentration Determination*

The concentration where LLPS was observed was assessed using the solvent shift method in the presence and absence of surfactant using UV extinction and ultracentrifugation (7). Flux measurements (15) were used for confirmation in select instances.

For UV-extinction, a methanolic stock solution of CPD was titrated into 15 ml of pH 6.8 phosphate buffer using a syringe pump (Harvard apparatus, Holliston, MA). The addition rate of the stock solution was adjusted such that the duration of the experiment was less than 10 min. The methanolic stock solution of CPD was prepared to be sufficiently concentrated such that final methanol content did not exceed 2%.

Measurements were undertaken at 37°C with stirring at 300 rpm. A UV/vis spectrophotometer coupled with a 1-cm path length fiber optically coupled dip probe (Tuscan, AZ, USA) were used to monitor changes in scattering by monitoring extinction at a non-absorbing wavelength (450 nm). The time interval between scans was 15 s. The concentration at which an increase in scattering was observed was taken as the amorphous solubility i.e. the LLPS onset. All experiments were repeated at least in triplicate.

The amorphous solubility was also assessed by centrifugation by adding 70–100  $\mu$ L of a concentrated methanolic stock solution of CPD (10–15 mg/ml) to 10 ml of buffer at 37°C to produce a solution with a concentration above the amorphous solubility. 1 ml of the resultant system was centrifuged at 14800 rpm (21100 g) for 45 min at 37°C using a Sorvall Micro 21R Microcentrifuge (ThermoFisher Scientific, Hanover park, IL) equipped with a 24  $\times$  1.5/2.0 ml rotor with click seal biocontainment lid, to pellet the drug-rich phase. Alternatively, if pelleting was incomplete due to formation of very small nanoparticles, an Optima L-100 XP ultracentrifuge equipped with a fixed-angle rotor 50.2 Ti (Beckman Coulter, Inc., Brea, CA) was used for centrifugation at 45000 rpm (184048 g) for 40 min at 37°C. An aliquot of 500  $\mu$ L of supernatant was diluted with 500  $\mu$ L of organic solvent (methanol:acetonitrile 30:20 v/v) followed by concentration determination using an Agilent 1260 Infinity high performance liquid chromatography (HPLC) system (Agilent Technologies, Santa Clara, CA). An Ascentis Express column (15 cm  $\times$  4.6 mm, 5  $\mu$ m) Sigma Aldrich (St. Louis, MO) was used for chromatographic separation. The mobile phase consisted of phosphoric acid 25 mM: methanol:acetonitrile (40:40:20 v/v) at a flow rate of 1 ml/min. The injection volume was 20  $\mu$ L and an ultraviolet (UV) detector at a wavelength of 220 nm was used to detect CPD.

#### *Determination of Surfactant Critical Micelle Concentration (CMC)*

Fluorescence spectroscopy was used to determine the CMC of surfactants SDS, CTAB and TPGS in 50 mM phosphate buffer at 37°C using pyrene as the environment sensitive fluorescent probe molecule. TWN did not present a clear CMC by fluorescence. In some cases, values were confirmed using surface tension measurements. At concentrations below the CMC, surfactants exist in solution as monomers and pyrene is molecularly dissolved in a hydrophilic aqueous environment. When the CMC is reached, surfactants form micelles with a lipophilic core whereby partitioned pyrene senses a less

polar environment. The slope change of the ratio of the emission peak at 371 nm, (peak I) to the peak at 382 nm (peak III) as a function of surfactant concentration enables the CMC to be determined (38).

The fluorescence spectrum for solutions containing 0.2 µg/ml pyrene was acquired as a function of surfactant concentration at 37°C using a Shimadzu RF-5301PC spectrofluorometer (Kyoto, Japan) at an excitation wavelength 332 nm. The emission wavelength at the maximum intensity  $\lambda_{\text{max}}$  350 nm was recorded and the concentration at which a change in the slope of the ratio of the emission peak at 371 nm, (peak I) to the peak at 382 nm (peak III) observed was taken as the CMC.

The surface tension of phosphate buffer at 37°C as a function of surfactant concentration was measured by the Wilhelmy method using a Kruss tensiometer (Hamburg, Germany). CMC was taken as the break point in a plot of surface tension *versus* log surfactant concentration.

#### Nanodroplet Size Stability

Drug-rich nanodroplets were formed following anti-solvent addition of a methanolic stock solution of CPD (10 mg/ml) to phosphate buffer, with or without surfactant, pre-equilibrated at 37°C. Samples were maintained at 37°C and 200 rpm over the 4-h experimental time period. The target particle concentration was  $10^8$ – $10^{10}$  particles/ml. The analysis temperature was maintained at 37°C during measurement.

Nanodroplet size was monitored every hour for 4 h in presence of surfactants using dynamic light scattering (DLS) performed with a Zetasizer Nano ZS (Malvern Instruments, Westborough, MA). The instrument was set to backscatter mode at an angle of 173°.

Size distribution and particle concentration were determined by nanoparticle tracking analysis (NTA) using a Nanosight LM10 (Malvern Instruments, Westborough, MA) equipped with a 532 nm laser. The light scattered by the nanodroplets were observed using a  $\times 20$  objective and 3 videos of 30 s each were recorded. All experiments were repeated in triplicate.

#### Zeta Potential Measurements

Zeta potential reflects the surface potential of the nanodroplets. Adsorption of surfactants onto the nanodroplet surface is expected to alter zeta potential, particularly for charged surfactants, leading to stabilization due to electrostatic repulsion (39). Zeta potential in

the presence of surfactants was determined using a Zetasizer Nano ZS (Malvern instruments, Westborough, MA). The temperature of the sample holder was set at 37°C.

#### Solution $^1\text{H}$ Nuclear Magnetic Resonance (NMR) Spectroscopy

A Bruker Avance-III-800 (Bruker BioSpin, Karlsruhe, Germany) equipped with a QCI cryoprobe was used for all NMR measurements. Two different sequences were used, WATERGATE and single pulse.

Phosphate buffer 50 mM pH 6.8 containing trimethylsilyl propionate (TSP) at 50 µg/ml as the internal reference standard was prepared in  $\text{H}_2\text{O}/\text{D}_2\text{O}$  (9/1, v/v). Surfactants were dissolved in the buffer at the desired concentration. CPD stock solutions at 10 mg/ml and 1 mg/ml were prepared in methanol- $\text{d}_4$ . The CPD stock solution was spiked into the buffer containing surfactant pre-equilibrated at 37°C stirring at 300 rpm. The concentration of methanol- $\text{d}_4$  added was always below 2% v/v. 500 µL of sample was transferred to an NMR tube and spectra were collected at 37°C or 50°C with suppression of water signal using the WATERGATE solvent suppression method (40). The scan number of spectra was set at 64 for SDS and CTAB solutions, and 128 for TPGS and TWN solutions.

For single pulse measurements, samples were prepared in pH 6.8 50 mM phosphate buffer containing 50 µg/ml TSP where  $\text{D}_2\text{O}$  was used instead of  $\text{H}_2\text{O}$ . The  $^1\text{H}$  NMR spectrum was obtained with a single pulse sequence using a relaxation delay of 15 s and the 90-degree high power pulse (P1) was 10.25 µs.

CPD and surfactant concentrations were determined from the peak area of the  $^1\text{H}$  NMR spectra using TSP as the internal reference.

#### Amorphous Solid Dispersion Preparation by Rotary Evaporation

CPD-PVPVA binary and CPD:PVPVA:surfactant ternary ASDs were prepared by rotary evaporation. The amount of surfactant in the ternary ASD was kept constant as 5 g of surfactant per 100 g of drug and polymer. Compositions of the ASDs are expressed as weight ratios rather than weight percent to enable easier comparison between the performance of binary *versus* ternary ASD. For example, CPD 40 drug loading (DL) refers to 40 g of CPD and 60 g of PVPVA for the binary ASD, while it refers to 40 g of CPD, 60 g of PVPVA, and 5 g of surfactant for the ternary system. ASDs with drug loadings from 20 to 60 DL and various surfactants (SDS, CTAB, TPGS and TWN) were prepared by dissolving solids in approximately 50 ml of methanol followed by 20 min sonication until a clear solution was obtained. Solvent

was removed by rotary evaporation using a Heidolph rotary evaporator (Schwabach, Germany) rotating at 150 rpm equipped with a Heidolph water bath maintained at 50°C. Samples were subsequently left under vacuum for at least 24 h. The ASD powder was milled using a mortar and pestle and sieved through a 425 µm sieve.

#### Surface Normalized Dissolution of ASD Tablets

Surface normalized dissolution under non-sink conditions with respect to the amorphous solubility was carried out using Wood's intrinsic dissolution rate apparatus (Agilent Technologies, Santa Clara, CA). Surface normalized dissolution assumes that the exposed surface area of the eroding tablet remains constant through the experiment. The ASD tablets were prepared immediately prior to release experiments by adding 100 mg of ASD powder into an 8 mm die yielding a tablet surface area of 50 mm<sup>2</sup>. The powder was tableted by applying a compression force of 1500 psi for 60 s using a manual Carver press (Carver Inc., Wabash IN). The die was mounted onto a shaft which was attached to an IKA Eurostart 20 overhead stirrer (IKA Works Inc., Wilmington, NC) and a rotation speed of 100 rpm was used. The die containing the tablet was immersed into 100 ml of 50 mM pH 6.8 phosphate buffer degassed and pre-equilibrated at 37°C in a water jacketed beaker. Sample was removed every 5 min for the initial 20 min and then every 10 min up to 120 min of analysis time. Fresh medium was added to maintain a constant volume.

Clopidogrel concentration was determined by HPLC using an Agilent 1100 system (Agilent Technologies, Santa Clara, CA). The column used for separation was a Thermo Hypersil gold C8 150 cmx 4.6 mm with 3 µm particle size column (Thermo Scientific, Waltham, MA). The mobile phase consisted of phosphoric acid 25 mM in water:methanol:acetonitrile 40:40:20 v/v/v pumped at 0.7 ml/min flow rate. The injection volume was 10 µL and retention time was 4.4 min. CPD was detected using an ultraviolet (UV) detector at a wavelength (λ) 217 nm. A calibration curve was build using CPD for the concentration range 5 to 80 µg/ml (r<sup>2</sup> of 0.999). All samples were diluted if needed using mobile phase to a concentration within the calibration curve range.

PVPVA concentration was assessed by HPLC using a size exclusion chromatography (SEC) column, 300 mm × 8 mm A 2500 Viscotek with an exclusion limit of 10000 Da for pullulan (Malvern Panalytical, Malvern, UK). The column temperature was 37°C. The mobile phase was composed of pH 7.4 phosphate-buffered saline: methanol 80:20 v/v at a flow rate of 0.5 ml/min. The injection volume was 40 µL and PVPVA was detected by UV absorption at a wavelength of 205 nm

and the retention time was 10.5 min. A calibration curve of PVPVA in the range 10 to 80 µg/ml was linear (r<sup>2</sup> of 0.999). Samples were diluted, if needed, with mobile phase to adjust concentrations to be within the calibration curve range.

The surface normalized dissolution rate (R) was calculated based on the mg released *versus* time profile. The slope from cumulative mg release vs time represents the dissolution rate (k). To normalize, k was divided by the tablet surface area (S, 0.5 cm<sup>2</sup>) multiplied by the fraction of the component (x) (Eq. 1)

$$R = \frac{k}{S \times x} \quad (1)$$

Statistical analysis for the percent release and the normalized release rate of the different ASDs was performed using RStudio software (41). Analysis of variances (ANOVA) was run followed by the post hoc test Turkey HSD to determine if differences were statistically significant.

#### Amorphous-Amorphous Phase Separation Determination by Fluorescence Microscopy

Confocal microscopy was used to investigate phase separation using Nile red and Alexa 488 as the hydrophobic and hydrophilic fluorescent probes, which are expected to stain the drug-rich and polymer-rich phases respectively. When phase separation occurs, forming drug-rich and polymer-rich phases, the hydrophobic probe will partition into the drug-rich phase, with a concurrent increase in signal while the hydrophilic probe will partition into the polymer-rich phase (12, 16, 42–44).

A thin ASD film containing the probes was prepared by spin coating using a Chemat Technology KW-4A spin coater (Northridge, CA). Samples were spincoated at 30 rpm for 12 s followed by 2000 rpm for 50 s, followed by heating at 70°C. To evaluate water-induced phase separation, freshly prepared films were compared to films exposed to 100% RH for 5 min. Films were observed using a Nikon A1R confocal microscope (Nikon Corporation, Tokyo, Japan) using an excitation wavelength at 561 nm for Nile red and 488 nm for Alexa 488.

## RESULTS

### Critical Micelle Concentration (CMC)

Table I shows the CMC values determined for the various surfactants, together with the hydrophilic-lipophilic balance (HLB) values from literature.

**Table I** Critical Micelle Concentration (CMC) of Surfactants by Fluorescence Spectroscopy (F) and in Some Cases Confirmed by Surface Tension (ST). CMCs were Determined in 50 mM Phosphate Buffer, pH 6.8 and 37°C

Surfactant	CMC ( $\mu\text{g/ml}$ )	Method	HLB
SDS	487 $\pm$ 34	F, ST	40 (45)
CTAB	50	F, ST	22 (46)
TPGS	40	F, ST	13.2 (47)
TWN	~14	ST	15 (45)

SDS has the highest CMC, whereby the measured value is in good agreement with literature reports for a similar medium (500  $\mu\text{g/ml}$  (5), and 433  $\mu\text{g/ml}$  (48)). The CMC value obtained for CTAB herein is lower than the value reported for in water (328  $\mu\text{g/ml}$ ) (49). TWN has a reported CMC value range from 13 to 34  $\mu\text{g/ml}$  in water (50–52) and 4.7  $\mu\text{g/ml}$  in 10 mM phosphate-buffered normal saline pH 7.4 at 25°C (53). The high variation in reported CMC for TWN is likely due to chemical heterogeneity and batch-to-batch variability (54, 55). The CMC of TWN obtained in this study falls within the range of the previously reported values. The CMC of TPGS in water at room temperature was reported as 30  $\mu\text{g/ml}$  (56) which is close to the experimental value in phosphate buffer noted in this study.

### Liquid-Liquid Phase Separation Concentration (LLPS)

The LLPS concentrations for CPD in various media are summarized in Table II. The impact of surfactant concentration on the LLPS concentration varied depending on the surfactant. SDS behaved as observed previously (5), where the LLPS concentration increased only when CMC was exceeded (Fig. S1). Solubilization, as reflected by an increase in the LLPS concentration was not observed for low TPGS and TWN concentrations (5  $\mu\text{g/ml}$ ), whereas increases were observed for higher surfactant concentrations (50  $\mu\text{g/ml}$ ). A lower LLPS concentration in  $\text{D}_2\text{O}$  versus  $\text{H}_2\text{O}$  PB has been reported previously (25), and can be attributed to the higher polarity of  $\text{D}_2\text{O}$ ;  $\text{D}_2\text{O}$  is reported to be more ordered and to form stronger hydrogen bonding compared to  $\text{H}_2\text{O}$  (57).

### Nanodroplet Size Stability

Increasing surfactant concentration resulted in CPD nanodroplets with a smaller initial size. For example, an initial size reduction from ~520 nm in buffer to 280 nm in the presence of 4  $\mu\text{g/ml}$  of TPGS was observed (supplementary information, section S2). Similar decreases

**Table II** LLPS Concentration of CPD in Different Media at 37°C. Reported Value Corresponds to UV-Extinction (UV) Method and were Confirmed Using Centrifugation (C) or Diffusion Cell (DC)

Solvent	LLPS concentration ( $\mu\text{g/ml}$ )	Method
Phosphate buffer pH 6.8	23 $\pm$ 3*	UV, C, DC
SDS 50 $\mu\text{g/ml}$	20 $\pm$ 1	UV, C
CTAB 5 $\mu\text{g/ml}$	20 $\pm$ 1	UV
CTAB 50 $\mu\text{g/ml}$	24 $\pm$ 2	UV
TPGS 5 $\mu\text{g/ml}$	20 $\pm$ 1	UV
TPGS 50 $\mu\text{g/ml}$	29 $\pm$ 2	UV
TWN 5 $\mu\text{g/ml}$	25 $\pm$ 2	UV, C
TWN 50 $\mu\text{g/ml}$	30 $\pm$ 2	UV, C
PB in $\text{D}_2\text{O}$ , pH 6.8	17 $\pm$ 1	UV
Water	49	UV

Reported values are mean  $\pm$  standard deviation for  $n=3$  from the UV method

\*value by UV extinction, confirmed by ultracentrifugation (18.3  $\pm$  1.0  $\mu\text{g/ml}$ ) and diffusion cell (20  $\mu\text{g/ml}$  - 25  $\mu\text{g/ml}$ )

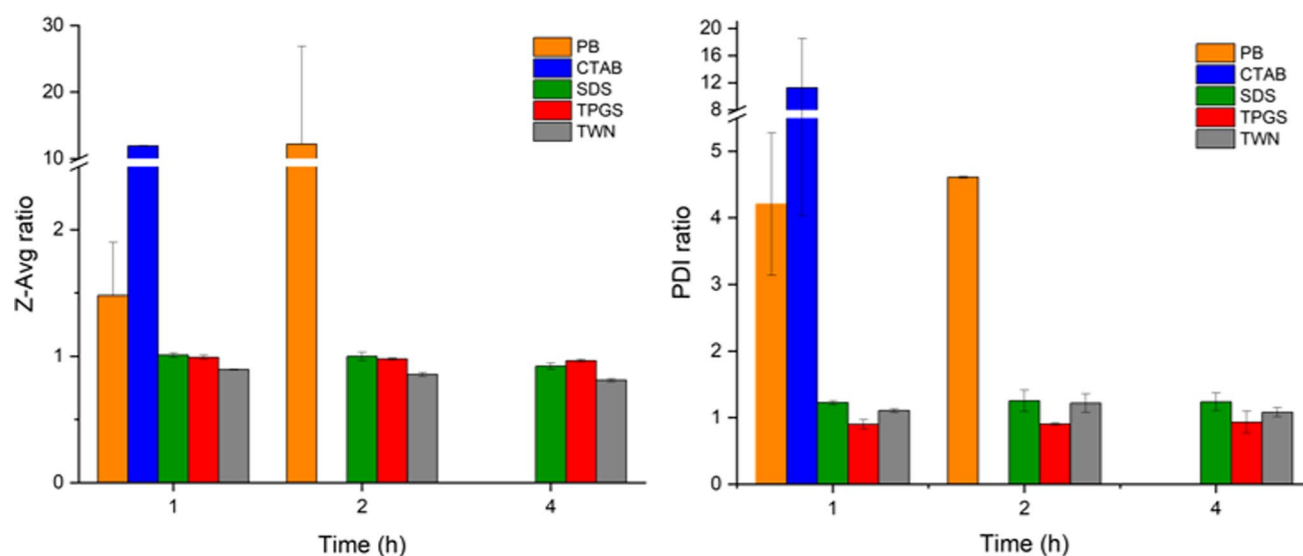
in size were observed for the other surfactants. The size stability of nanodroplets in the presence of different surfactants was also evaluated using DLS and NTA to identify the minimum amount of surfactant needed to prevent size enlargement (supplementary information, section S2). CPD nanodroplets were unstable in buffer, increasing in size and polydispersity index (Fig. 2). The surfactant concentration needed to stabilize nanodroplet size varied with surfactant type (Fig. 2). For example, 50  $\mu\text{g/ml}$  of SDS was necessary to stabilize the nanodroplet size whereas  $\leq 5$   $\mu\text{g/ml}$  of TPGS and TWN was sufficient. In contrast, CTAB induced instability, producing large agglomerates that floated on the solution surface (supplementary information, section S2).

Figure 3 presents results for zeta potential measurements of CPD nanodroplets in the presence and absence of the different surfactants.

The increase in the absolute magnitude of the zeta potential by SDS and CTAB, and the decrease in the presence of TWN and TPGS support adsorption of the surfactant at the nanodroplet surface.

### $^1\text{H}$ NMR Spectroscopy

Peaks arising from aromatic groups in CPD, with assignments are shown in Fig. 4. At 37°C, only peaks arising from molecularly dissolved CPD were visible, despite the presence of nanodroplets. When the temperature was increased to 50°C, a second set of CPD aromatic proton peaks was observed, arising from clopidogrel present in drug-rich nanodroplets. Additionally, at 50°C solubility was increased to ~30  $\mu\text{g/ml}$ , thus at the evaluated temperature, ~40  $\mu\text{g/ml}$  of CPD is in the drug-rich



**Fig. 2** CPD nanodroplet size stability at 37°C in 50 mM PB pH 6.8 without surfactant and with CTAB at 50  $\mu\text{g/ml}$ , SDS at 50  $\mu\text{g/ml}$ , TPGS at 4  $\mu\text{g/ml}$ , and TWN at 5  $\mu\text{g/ml}$ . **(a)** Z-Average ratio and **(b)** PDI ratio. Size stability also confirmed by NTA. The ratio was calculated by dividing the property at the experimental time point by the corresponding value at  $t=0$ . A ratio close to 1 indicates no change in the parameter, while values  $>1$  indicate particle size/polydispersity increase. Values are mean  $\pm$  standard deviation for  $n=3$ .

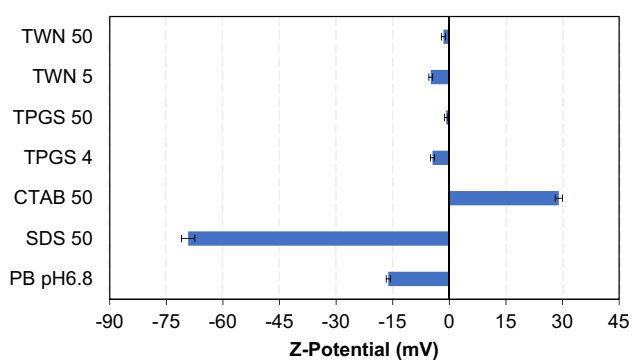
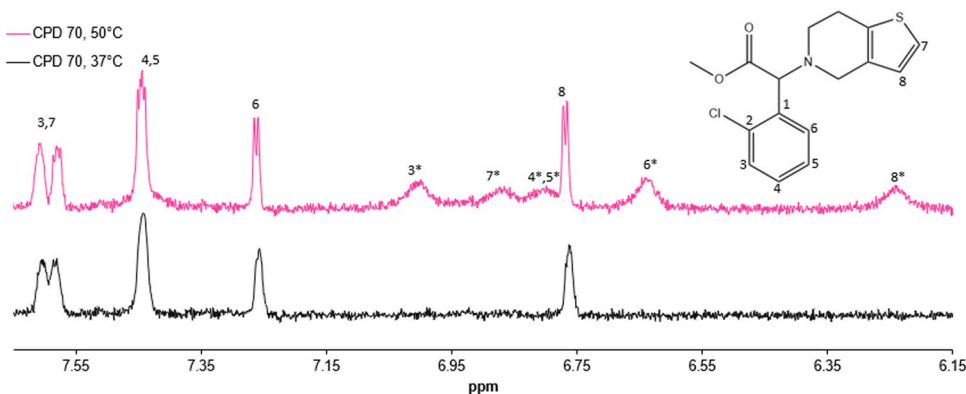


**Fig. 3** Zeta potential of clopidogrel at 70  $\mu\text{g/ml}$  (50  $\mu\text{g/ml}$  as nanodroplets) in 50 mM phosphate buffer without surfactant (PB pH 6.8) and with surfactants: SDS at 50  $\mu\text{g/ml}$  (SDS 50), CTAB at 50  $\mu\text{g/ml}$  (CTAB 50), TPGS at 4 and 50  $\mu\text{g/ml}$  (TPGS 4, TPGS 50), and Tween 80 at 5 and 50  $\mu\text{g/ml}$  (TWN 5, TWN 50). Values are mean  $\pm$  standard deviation for  $n=3$ .

nanodroplet phase. Peaks arising from CPD in the drug-rich nanodroplets were broad and up-field from the peaks arising from molecularly dissolved CPD, consistent with the molecules in the nanodroplets experiencing a less polar and lower mobility environment than the clopidogrel molecules dissolved in water. Similar observations have been made for the NMR spectra of ibuprofen solutions at concentrations above the amorphous solubility. In these spectra, there are two sets of peaks which arise from molecularly dissolved drug and drug in the drug-rich nanodroplets, whereas below the LLPS concentration, only one set of peaks was present (58). The appearance of the CPD nanodroplet peaks at 50°C (but not at 37°C) is due to the increased mobility of the molecules in the drug-rich nanodroplets as the temperature is increased, whereby the reorientation

**Fig. 4** CPD in 50 mM PB pH 6.8 at 37°C (black) and at 50°C (pink). New peaks detected at 50°C (marked with \*) correspond to CPD in the nanodroplet phase. The CPD concentration was 70  $\mu\text{g/ml}$ .





correlation time of CPD molecules in the nanodroplets now becomes fast enough to be captured by solution-state NMR spectroscopy (25). This phenomenon has been reported previously for amorphous indomethacin. Static proton NMR of amorphous indomethacin showed solution-like sharp peaks corresponding to the supercooled liquid form of indomethacin when measured at 90°C which is around 50°C higher than the indomethacin  $T_g$  (onset at 42°C); however, at temperatures close to the  $T_g$  (50°C and 70°C), indomethacin peaks were substantially broadened (59). The  $T_g$  of CPD is -9°C and clearly molecular mobility is insufficient at 37°C, but becomes high enough to detect the drug in the drug-rich nanodroplets at 50°C. As expected, nanodroplet peaks were absent from NMR spectra of solutions below the LLPS concentration, and the intensity of the peaks assigned to drug in the nanodroplets increased with an increasing concentration of nanodroplets (supplementary information, section S3).

NMR spectroscopy can be used to obtain information on micellar solubilization by measuring shifts in peak positions on addition of the solute to a solution containing the surfactant. For example, the  $^1\text{H}$  NMR spectrum of a compound solubilized in a surfactant typically shows an up-field shift consistent with a less polar environment (32). NMR spectroscopy can also be used to determine if additives such as surfactants become depleted from solution due to partitioning into

drug-rich nanodroplets (60–62). Representative NMR spectra are shown below for the TPGS system which shows evidence of both micellar solubilization of the drug as well as partitioning of the surfactant into the drug-rich nanodroplets.

Figure 5 shows that CPD solution-phase peaks are shifted up-field in the presence of TPGS. The shift was observed for CPD concentrations both above and below the LLPS concentration (supplementary information, section S3). This suggests a solution phase interaction, namely solubilization in micelles. The environment in the micelles is less polar relative to water, accounting for the up-field shift. Although TPGS CMC in buffer is ~50 µg/ml, it is well known that the presence of additives (for example a drug) affects the CMC (63, 64).

In concert, TPGS peaks shifted up-field in the presence of CPD. This suggests that the chemical environment around TPGS was changed, thus surfactant molecules experience a less polar environment. Additional experiments were conducted to evaluate depletion of TPGS from the solution phase and confirm partitioning into the nanodroplets. A single pulse sequence was used to accurately quantify TPGS since the NMR peak area is less affected by J-modulation and T relaxation effects (65–67). Experiments were also conducted at 50°C to interrogate CPD nanodroplets.

At 50°C, CPD solution phase peaks are broadened and up-field-shifted in the presence of TPGS (as

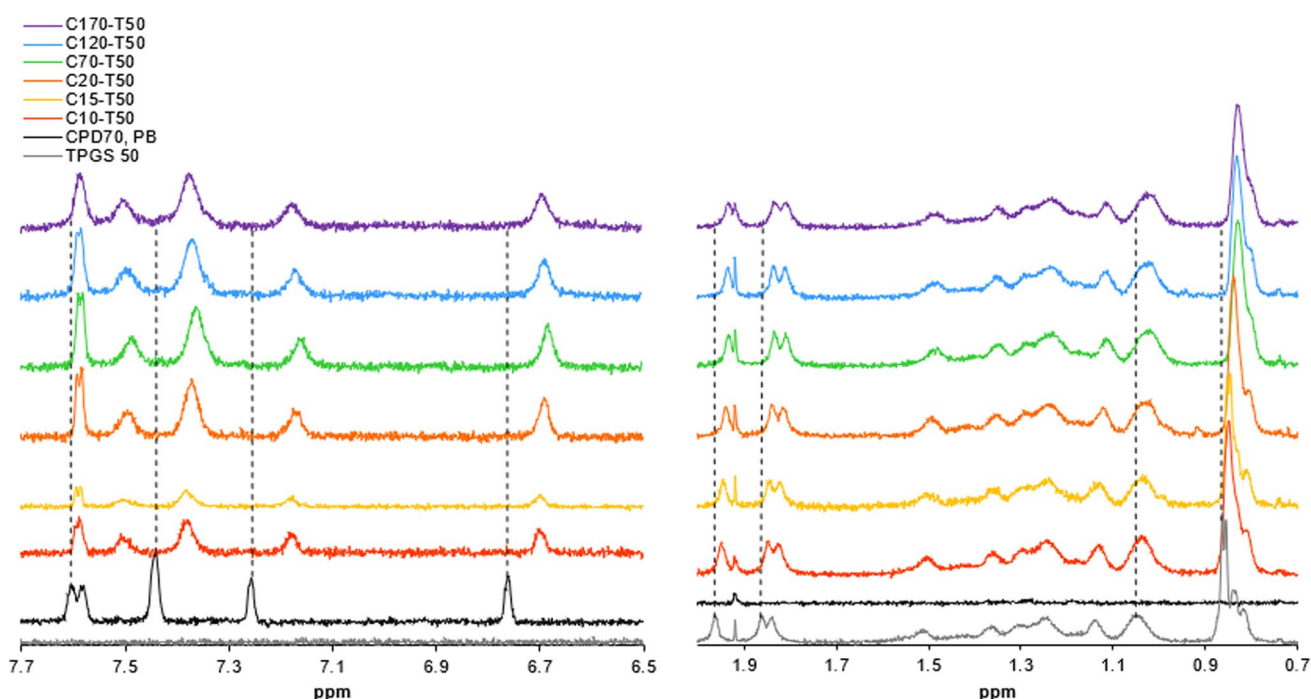


**Fig. 5** Clopidogrel (left) and TPGS (right) peaks for increasing concentrations of CPD at 37°C in 50 mM PB pH 6.8 containing TPGS at 50 µg/ml. Vertical dashed lines correspond to CPD and TPGS peak position in buffer. Legend shows the clopidogrel (C) and TPGS (T) concentrations in µg/ml.

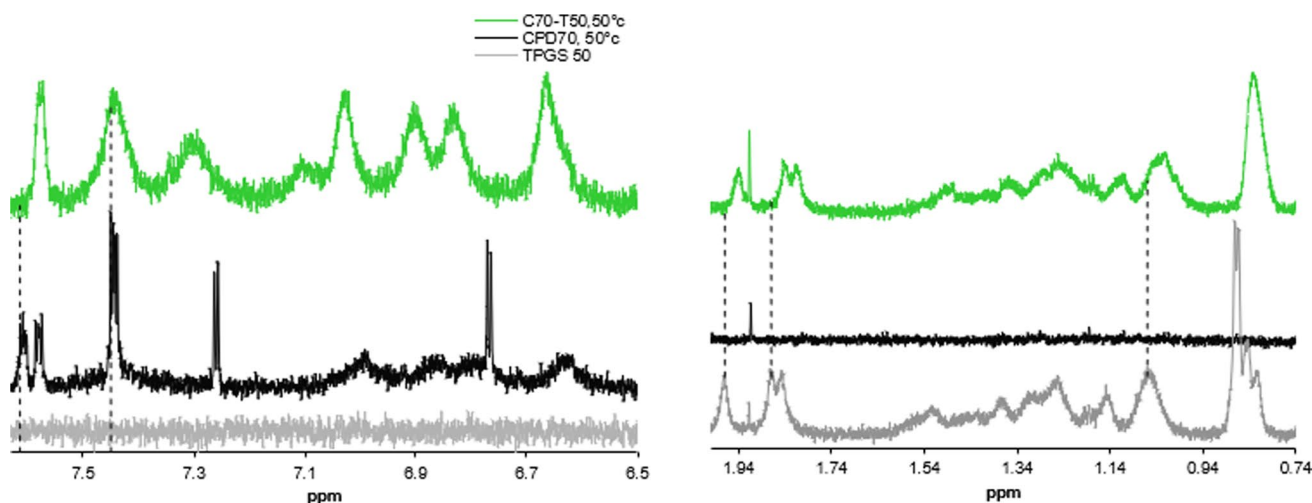


**Fig. 6** Clopidogrel (left) and TPGS (right) peaks for CPD 70  $\mu\text{g}/\text{ml}$  and TPGS 50  $\mu\text{g}/\text{ml}$  at 50°C in 50 mM PB pH 6.8. Vertical dashed lines correspond to CPD and TPGS peak position in buffer. Legend shows the clopidogrel (C) and TPGS (T) concentrations in  $\mu\text{g}/\text{ml}$ .

seen at 37°C) while nanodroplet peaks are downfield shifted and more intense (Fig. 6). The down-field shift of the CPD nanodroplet peaks suggests that some TPGS is partitioning into the nanodroplets, leading to a more polar environment for the drug molecules in this phase, and increased mobility, producing sharper peaks, as a result of surfactant incorporation.

Integration of select TPGS peaks indicated that the concentration of TPGS in the aqueous phase decreased from 50  $\mu\text{g}/\text{ml}$  to 33  $\mu\text{g}/\text{ml} \pm 5.4 \mu\text{g}/\text{ml}$  in the presence of CPD nanodroplets (CPD concentration of 70  $\mu\text{g}/\text{ml}$ ). The peaks from the TPGS that distributed into CPD nanodroplets were not detected by solution-state NMR due to the high viscosity environment of CPD nanodroplets reducing the peak signal of TPGS. The suggested composition of the

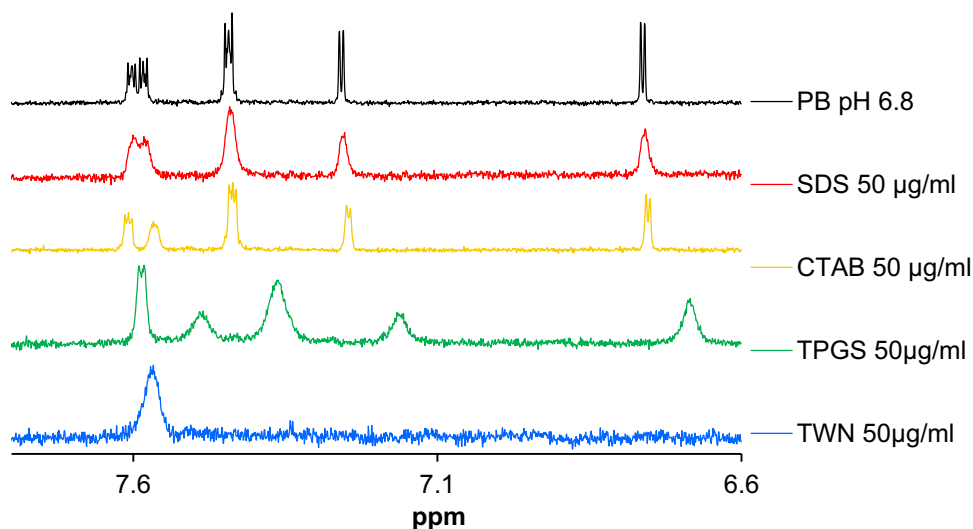
nanodroplets was 50:17 w/w CPD:TPGS for this system. Incorporation of TPGS into CPD nanodroplets was confirmed using HPLC analysis of supernatant concentrations after pelleting of nanodroplets (supplementary information, section S3).

Figure 7 and Table III summarize the changes in the NMR spectra in the presence of each of the surfactants and the underlying interpretation. Further details are found in the supplementary information (Figs. S6–16).

### Surface Normalized Dissolution

Surface normalized dissolution profiles for various CPD-PVPVA ASDs with and without additional 5% surfactant are shown in Fig. 8. At DLs of 40 and 50 wt.%, all of the ASDs release sufficient drug such that the LLPS

**Fig. 7** Clopidogrel peaks for CPD 70  $\mu\text{g}/\text{ml}$  in 50 mM phosphate buffer pH 6.8 (PB) and in the presence of 50  $\mu\text{g}/\text{ml}$  of SDS, CTAB, TPGS, or Tween@80 (TWN).



**Table III** Changes in the Spectra for CPD 70 µg/ml in the Presence of Surfactants

Surfactant 50 µg/ml	CPD in solution	CPD nanodroplets
SDS	No interactions	No interaction
CTAB	Incorporation into surfactant micelles	No interaction
TPGS	Incorporation into surfactant micelles	TPGS partition into CPD nanodroplets
TWN	Strong interaction	Minor partition of TWN into nanodroplets

concentration is exceeded within the first 10 min. However, release is incomplete, with a maximum of 80% drug being released for the best performing ASDs. Drug and polymer were observed to release nearly congruently for the 40% DL systems (Fig. 8a-e). However, the polymer release rate was slightly faster than that of the drug, especially at later time points. Given that more polymer is released than drug, the material remaining in the die is enriched in drug relative to the original formulation. This likely accounts for the incomplete release; when the release becomes drug-controlled, there is no driving force for drug dissolution if the concentration in solution is above the drug amorphous solubility. For CTAB-containing ASDs, drug loss from solution was seen after partial release, and this can be attributed to the surfactant causing agglomeration of the CPD nanodroplets; no evidence of crystallization was observed by polarized microscopy. This observation is in agreement with the DLS studies described above where CTAB was noted to result in rapid size enlargement of the CPD-rich dispersed phase. At 50% DL, PVPVA clearly released more rapidly than CPD in all the cases except for when SDS was included in the formulation, where close to congruent release of drug and polymer was observed.

Figure 9 summarizes the percentage release after 60 min as well as the normalized initial release rate (calculated from the initial data points where the release *versus* time profile is linear) for ASDs with a DL of 40–60%. The extent of drug release declines with DL, with a more drastic drop from 50 to 60% DL relative to from 40 to 50% DL. In contrast, PVPVA releases almost completely, regardless of drug load. Only SDS produced a statistically significant increase in the total percent release of CPD for the 50% DL relative to the ASD with no surfactant.

The normalized release rates of CPD and PVPVA were similar at 40% and 50% DL, although the polymer release generally trended higher than the drug release. In contrast, at 60% DL, PVPVA release was up to 10 times faster than that of CPD. Surprisingly, in binary dispersions, CPD increased the normalized release rate of PVPVA by a factor of approximately 2 relative to the release rate of neat polymer (Fig. 9d-f). Given the nearly

congruent release of the drug and polymer at 40% DL, this led to a very rapid release of the drug. While the rapid polymer release was maintained in the presence of SDS and CTAB, TPGS and TWN generally resulted in a similar polymer release rate as for the neat polymer, with the exception of the 60% DL TPGS ASD.

Addition of surfactant to the ASD generally led to the formation of somewhat smaller nanodroplets with a more uniform size distribution (smaller PDI) following dissolution (Fig. 10), in particular for the 50% DL ASDs. However, the presence of CTAB in the formulation induces nanodroplet coarsening producing larger species with a wider size distribution. These results are consistent with the size stability study described above.

### Amorphous-Amorphous Phase Separation by Confocal Microscopy

Evaluation of amorphous amorphous phase separation was carried out by confocal microscopy. Previous studies have suggested that the morphology of phase separated domains may impact drug release (68, 69). For these studies, ASD films containing Nile red and Alexa 488 were used. Nile red is a hydrophobic dye and Alexa 488 is a hydrophilic dye whose fluorescence intensities are strongly influenced by the polarity of their environment. If phase separation occurs, Nile red is expected to partition into the drug phase, leading to more intense and non-uniform emission (70, 71) while Alexa 488 is expected to partition into the polymer-rich phase due to its more hydrophilic nature (72, 73).

At 50% DL, after 5 min of exposure at 100% RH, phase separation was obvious where a bicontinuous structure was formed. (Fig. 11e, f). In contrast, the 40% DL film remains similar before and after exposure to high RH (Fig. 11a and d). For the 60% DL film, phase separation is also observed, whereby the drug appears to form the continuous phase, while the polymer is present as the discrete phase. These results are consistent with the release profiles. CPD 50% DL and above have non-congruent release with a higher percent release and faster dissolution rate for PVPVA relative to CPD (Fig. 11c and f), which in line with previous

**Fig. 8** Release profiles for CPD 40% DL (a) in the presence of surfactants: TWN (b), TPGS (c), SDS (d), and CTAB (e) and CPD 50%DL (f) in the presence of surfactants: TWN (g), TPGS (h), SDS (i), and CTAB (j). Values are mean  $\pm$  standard deviation for n = 3.

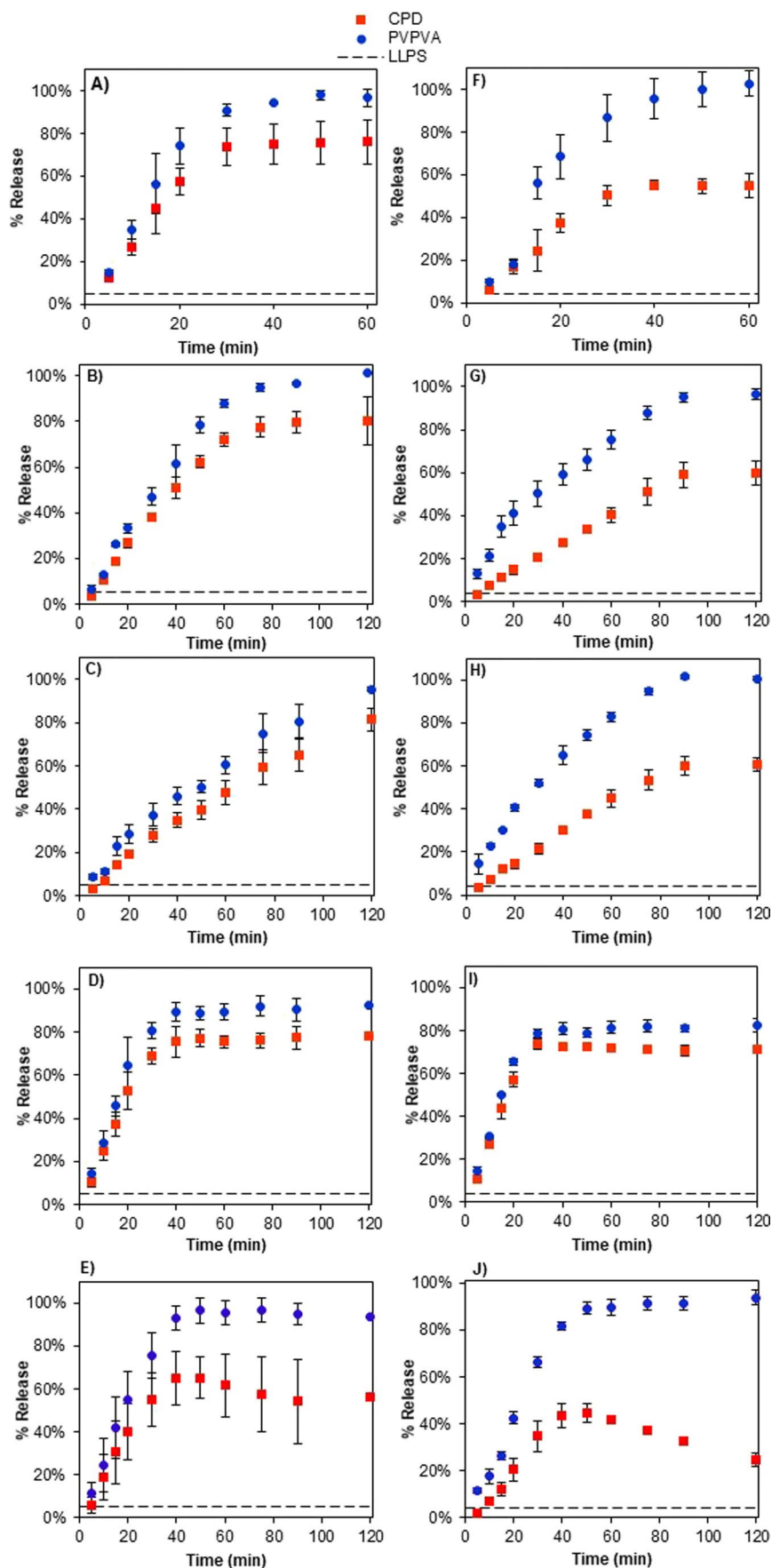


**Fig. 9** Total percent release (a-c) and normalized release rate (d-f) of CPD-PVPVA ASDs with and without surfactant at drug loadings 40% (a, d), 50% (b, e), and 60% (c, f). Values are mean  $\pm$  standard deviation for  $n=3$ . \* Statistically different compared to the corresponding binary ASD, with at least  $P<0.05$  in ANOVA and Tukey's HSD test. \* red for CPD and \* blue for PVPVA.

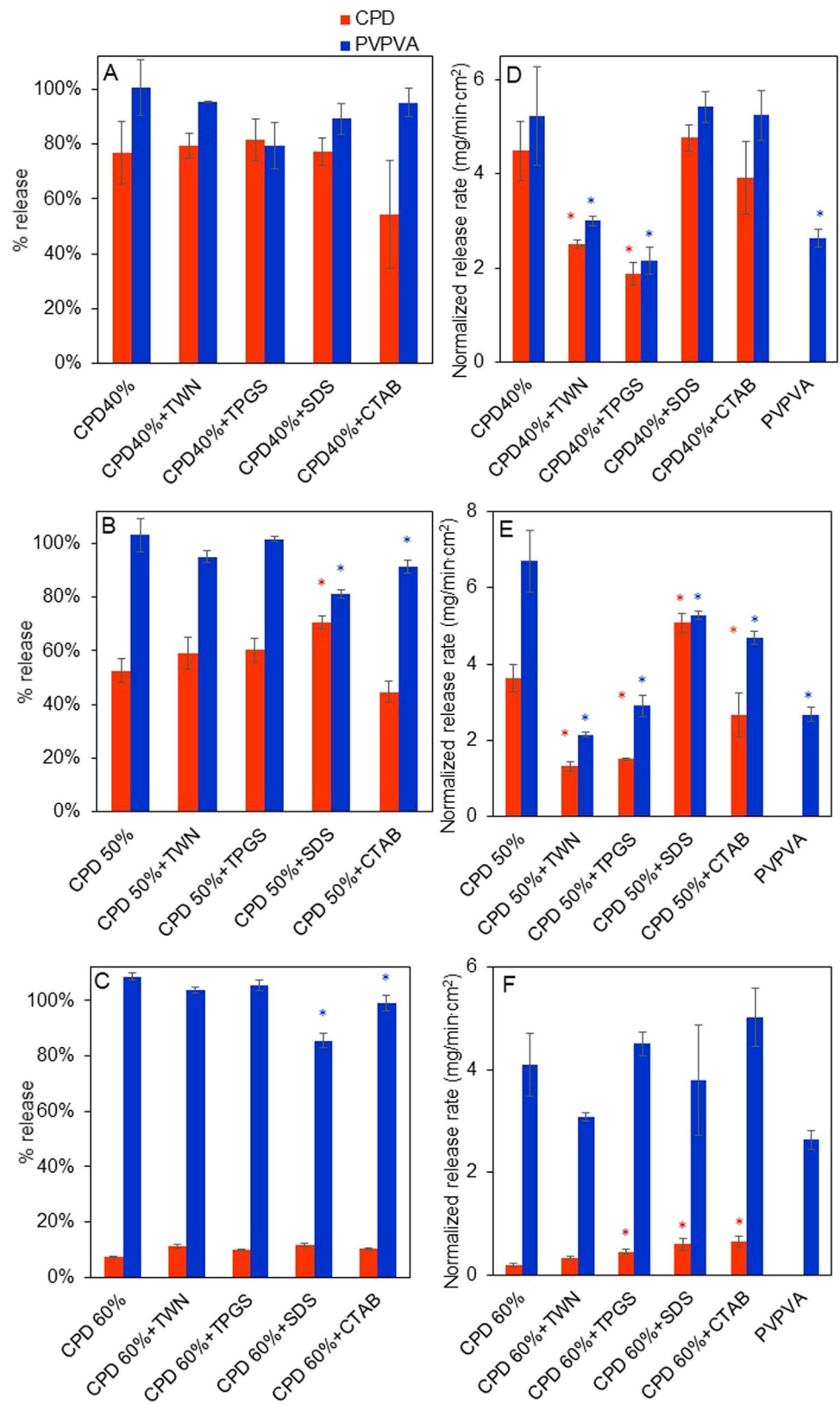


**Fig. 10** Nanodroplet size (Z-Average) measured by DLS at 90 min of dissolution of ASDs in the presence of different surfactants at 40%DL (a) and 50%DL (b). Values are mean  $\pm$  standard deviation for  $n=3$ .

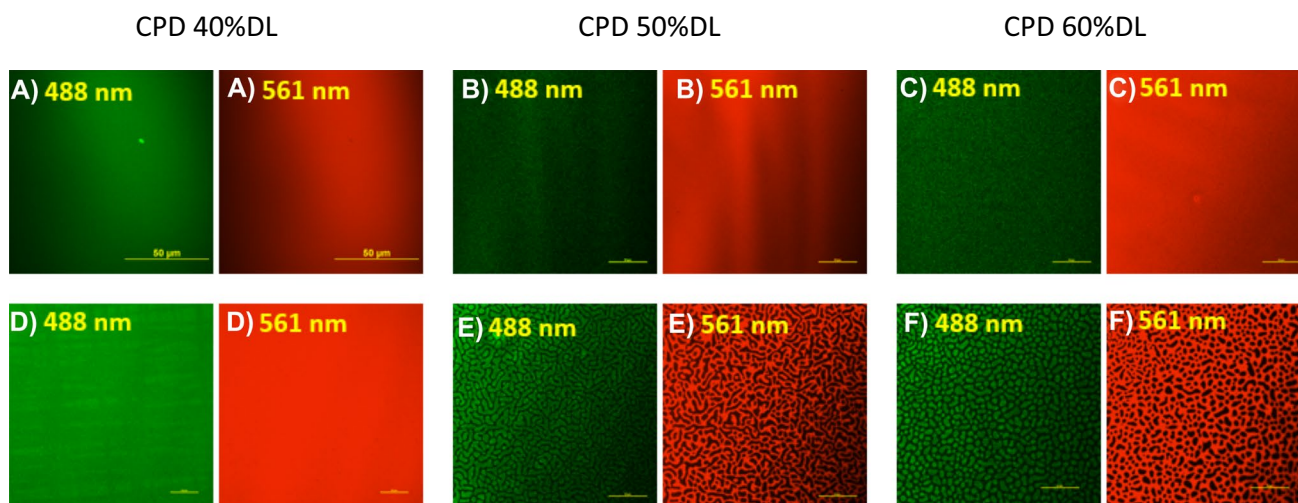
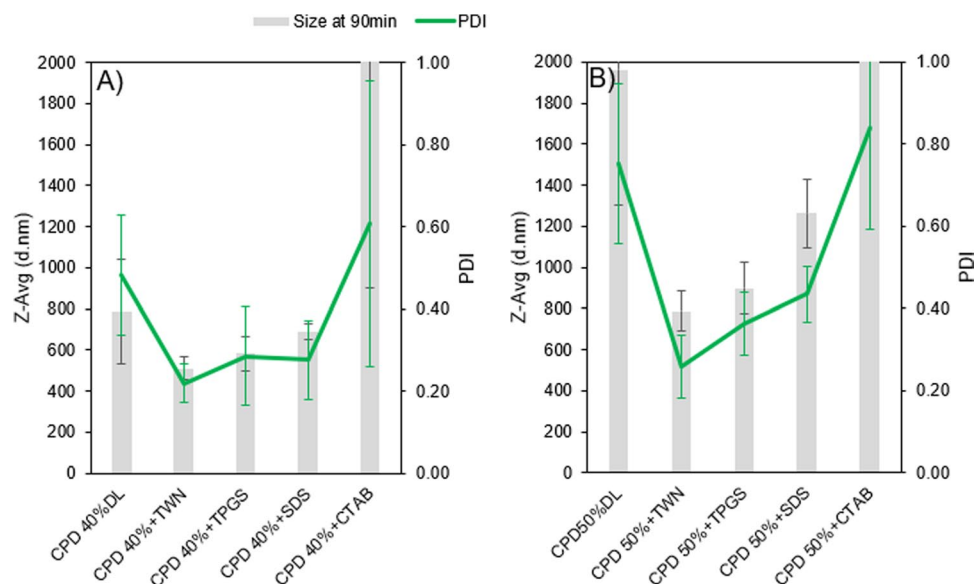


**Fig. 11** Confocal fluorescence microscopy images of 40% (a and d), 50% (b and e), and 60% (c and f) drug loading CPD:PVPVA ASD films before (a, b, c respectively) and after (d, e, f) exposure at 100% relative humidity for 5 min. Images acquired following excitation at 488 nm (Alexa 488) and 561 nm (Nile red). Scale bar is 50  $\mu$ m.

observations where continuous drug-rich phases correlated with poor release (68).

Ternary ASD-films at 50% DL and 60% DL films developed some variations in fluorescence intensity after exposure to high RH indicating phase separation. For the 50% DL ASD with SDS (Fig. 12), the film only shows a small extent of heterogeneity in fluorescence intensity, which becomes more pronounced for the 60% DL film. The CPD-rich phase forms the continuous phase at 60% DL in the presence of SDS, whereby the polymer-rich discrete phase is smaller than for the corresponding ASD in the absence of the surfactant. For TPGS-containing ASDs (Fig. 13), a

bicontinuous morphology is observed at 50% DL after high RH exposure, whereas at the 60% DL, more complex structures develop, suggesting more extensive coarsening of the two phases. For ASDs with TWN, a bicontinuous morphology was observed for DLs above 50% (Fig. 14).

## DISCUSSION

It has been suggested that the formation of nanodroplets during ASD dissolution may be beneficial for oral

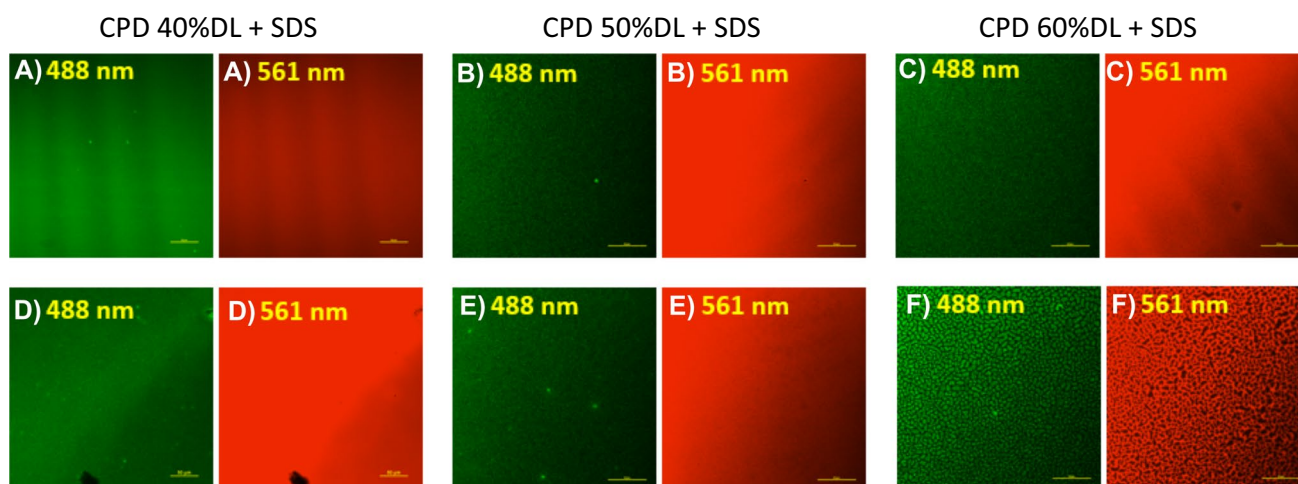


**Fig. 12** Confocal fluorescence microscopy images of 40% (a and d), 50% (b and e), and 60% (c and f) drug loading CPD:PVPVA ASD films containing 5% of SDS, before (a, b, c respectively) and after (d, e, f) exposure at 100% relative humidity for 5 min. Images acquired following excitation at 488 nm (Alexa 488) and 561 nm (Nile red). Scale bar is 50  $\mu$ m.

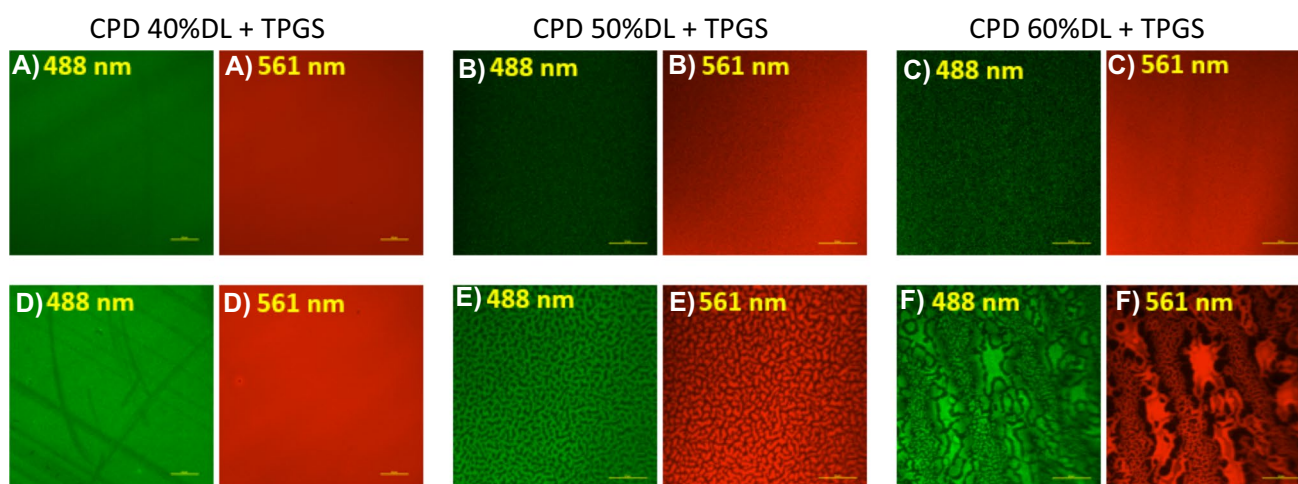


**Fig. 13** Confocal fluorescence microscopy images of 40% (a and d), 50% (b and e), and 60% (c and f) drug loading CPD:PVPVA ASD films containing 5% of TPGS, before (a, b, c respectively) and after (d, e, f) exposure at 100% relative humidity for 5 min. Images acquired following excitation at 488 nm (Alexa 488) and 561 nm (Nile red). Scale bar is 50  $\mu$ m.

bioavailability. (3, 11, 19–21) Therefore, it is of interest to develop ASD formulations that generate size-stable nanodroplets. In addition, there is also of interest to develop ASDs with high drug loadings, to minimize the patient pill burden by reducing the excipient load. However, high drug loading ASDs show a reduced tendency to form nanodroplets upon dissolution and typically have poor release (16). It has been suggested that the poor release occurs when the dissolving surface becomes enriched in drug. When this happens, the drug, rather than the polymer controls the drug release, and consequently, the release rate decreases (16). Consequently, the incorporation of excipients such as surfactants into ASD formulations is an active

area of exploration as an approach to manipulate nanodroplet size and stability, as well as to improve drug release from ASDs at high drug loadings.

#### Liquid-Liquid Phase Separation and Impact of Surfactants

It is well known that many drugs form amorphous nanodroplets when a certain concentration, corresponding to miscibility limit of the amorphous form of the drug with water, is exceeded. CPD shows clear evidence of the formation of a new phase when a concentration of  $\sim 23$   $\mu$ g/ml is exceeded. Furthermore, CPD is one of the few drugs where the  $^1\text{H}$  NMR spectrum of both drug species, namely molecularly dissolved drug and

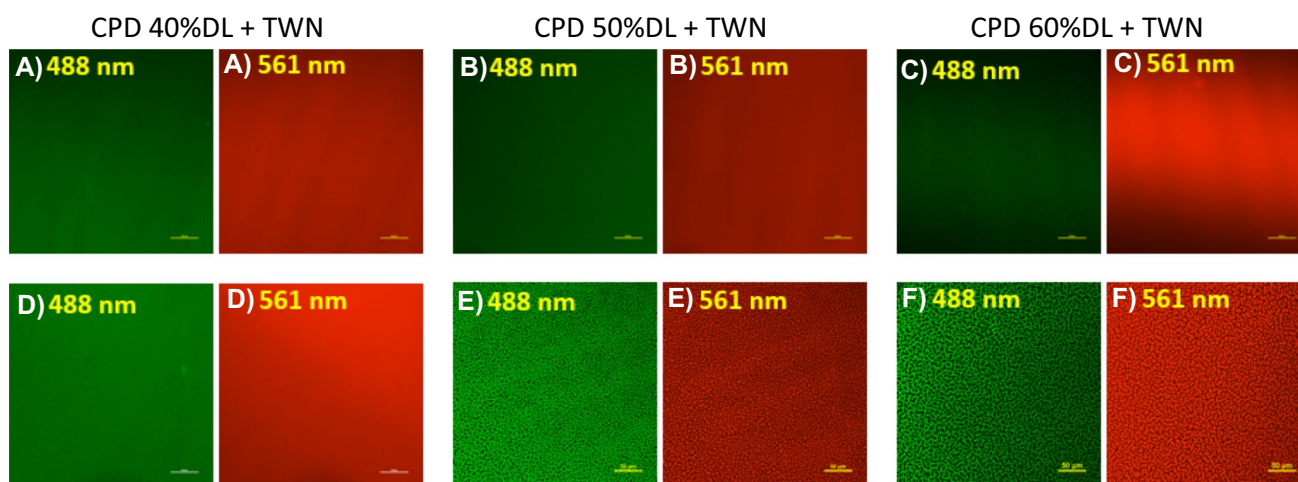


**Fig. 14** Confocal fluorescence microscopy images of 40% (a and d), 50% (b and e), and 60% (c and f) drug loading CPD:PVPVA ASD films containing 5% of TWN, before (a, b, c respectively) and after (d, e, f) exposure at 100% relative humidity for 5 min. Images acquired following excitation at 488 nm (Alexa 488) and 561 nm (Nile red). Scale bar is 50  $\mu\text{m}$ .

drug in the drug-rich nanodroplets, can be evaluated, as demonstrated in Fig. 4. Ueda et al., reported a direct evaluation of ibuprofen present in drug-rich amorphous nanodroplets by NMR. The direct evaluation was possible due to the low  $T_g$  ( $-45^\circ\text{C}$ ) of IBP relative to the experimental temperature ( $37^\circ\text{C}$ ), and the consequent high mobility of the molecules in the drug-rich phase (25). The low  $T_g$  of clopidogrel enables nanodroplet peaks to be detected when the temperature is elevated to  $50^\circ\text{C}$  and the molecular mobility is sufficiently increased. The NMR spectra provide insight into the environment of the CPD molecules in the two different phases. Not unexpectedly, the aqueous phase molecularly dissolved peaks are down-field shifted relative to those arising from drug in the drug-rich phase, consistent with a lower degree of shielding caused by interaction of molecularly dissolved CPD molecules with water. Light scattering experiments show that the dispersed phase rapidly coarsens in the absence of surfactants, consistent with the high interfacial energy of the lipophilic CPD-rich phase. Addition of surfactants, in general, was an effective approach to reduce the coarsening rate of the drug-rich nanodroplets formed by LLPS, leading to the observation of smaller species. CTAB provided an exception to this trend, promoting rapid size enlargement of the nanodroplets by an unknown mechanism. Surfactants were found to be effective at very low concentrations, which is a favorable finding in terms of including them in formulations, where constraints imposed by toxicity concerns and formulation design limit the amount of surfactant that can be used. The low effective concentrations are consistent with nanodroplet stabilization by surfactant adsorption at the droplet surface with resultant steric and/

or electrostatic stabilization. This scenario is exemplified by SDS where minimal SDS depletion was observed from aqueous phase, but an increased negative charge was observed in the presence of this surfactant. The non-ionic surfactants showed more complex interactions with CPD based on NMR spectroscopy, including partitioning into the nanodroplets in the case of TPGS. However, this behavior does not appear to be related to nanodroplet stabilization, and likely reflects the lower polarity of the non-ionic surfactants which promotes interaction with the drug-rich phase.

It is likely desirable to minimize the amount of surfactant used in the formulation, hence it is useful to know the minimum surfactant concentration required to prevent droplet size enlargement. The minimum concentration of surfactant needed to cover the surface of the nanodroplets can be estimated using values for the hydrodynamic radius ( $R_H$ ) obtained from DLS and NTA measurements, which in turn are used to estimate the droplet surface areas. Values for the molecular surface area of the surfactants are available from the literature. Calculations are presented in the supplemental information and the results are summarized in Table IV. For the non-ionic surfactants, reasonable agreement is observed between the theoretical monolayer surface coverage and the experimental effective concentration. For the ionic surfactants, CTAB was ineffective at inhibiting coarsening, even when tested at a concentration higher than the theoretical minimum concentration. For SDS, the higher effective experimental value most likely reflects the high HLB value for this surfactant, and a lower tendency to associate at the interface relative to the non-ionic surfactants, consistent with the higher CMC value of SDS.



**Table IV** Calculated Monolayer Concentration of Surfactant, and Experimentally Observed Minimum Effective Concentration to Prevent Droplet Coarsening. Surfactant Molecular Surface Areas (SAs) were Taken from the Literature

Surfactant	SA(Å <sup>2</sup> )*	Calculated monolayer coverage (µg/ml)	minimum effective surfactant concentration (µg/ml)
SDS	6.7–425 (74, 75)	0.3–17.8	50
CTAB	61.6 (76)	2.4	Not stable
TPGS	60 (20)	10.4	4
TWN 80	174 (54)	3.1	5

\*Values obtained from literature

The stabilization of the CPD disperse phase by the surfactants is promising in terms of exploiting the high surface area of the nanodroplets to maintain equilibrium with molecularly dissolved drug as the latter is absorbed across the membrane, which has been suggested to be beneficial for maintaining membrane transport at a maximized value (3). However, surfactants with properties similar to CTAB that induce droplet coarsening would be a poor choice for ASD formulations. Therefore, this type of surfactant screening may be useful when selecting surfactants for incorporation into ASD formulations; nanodroplets are generated during the dissolution of some amorphous solid dispersion formulations. Having evaluated CPD nanodroplet stability in the absence of a formulation, it is relevant to consider the generation and colloidal stability of CPD nanodroplets generated from an ASD with and without a surfactant, to determine if similar patterns of behavior are observed as for the solution screening studies.

### Release as a Function of Drug Loading

PVPVA is widely used in the commercial manufacture of ASD formulations, whereby its choice as an ASD polymer stems from its good processability (amenable to both spray drying and hot melt extrusion), as well as the high aqueous solubility. Intrinsic dissolution rate measurements have shown that neat PVPVA has a faster release rate than many other commonly used ASD polymers (77, 78). This rapid release rate translates to improved ASD dissolution performance, where several studies have demonstrated that, for low drug loading ASDs, the normalized release rate of the drug is the same as that of PVPVA, i.e. both components release congruently, and a similar normalized rate to that of the neat polymer. This has been termed the polymer-controlled regime. Under non-sink dissolution conditions, when release is rapid and congruent, drug-rich nanodroplets are generated, whereby these species are potentially beneficial to enhance oral bioavailability (3, 11, 79, 80). Consequently, formulating an ASD with polymer-controlled release is considered optimum.

However, it appears that for PVPVA-based dispersions, there is a maximum drug loading where release is polymer-controlled. Above this DL, the release rate of the two components diverges, and the drug release becomes very low and incomplete. (12, 16, 81) This drug loading limit where the drug release “falls-off-the-cliff” has been termed the limit of congruency (LoC), and, using surface normalized dissolution studies, has been found to range from <5% to ~30% DL for the various drugs studied to date. For example, the LoC for ledipasvir was reported to be 5% (12), nivaldipine and cilnidipine had values of around 10% and 15% respectively (81) while ritonavir was 25% (16). For the CPD binary ASDs, the LoC appears to be ~40%. Compared to the other PVPVA ASDs discussed above, this is a high LoC, although close examination suggests that the polymer is released slightly faster than the drug, which may explain why only ~80% drug is released. Further, the normalized release rate of PVPVA is enhanced by the addition of CPD, in particular for the binary ASDs (Fig. 9) relative to that of the neat polymer.

Thus, the CPD-PVPVA dispersions show a higher LoC than other systems studied to date, where close-to-congruent release is seen up to 40% DL (Figs. 8 and 9), and drug-rich nanodroplets are present in solution. At a 60% DL, the drug release has clearly fallen off the cliff, with minimal release, albeit rapid polymer dissolution. The high LoC observed for CPD likely arises as result of two properties of the drug. First, the very low  $T_g$  of the compound, and second, the lack of specific interactions with the polymer. It is well known that polymer dissolution rate is impacted by the  $T_g$  of the matrix relative to the dissolution temperature (82, 83). Several previous studies highlight the apparent role of  $T_g$  in the release performance of PVPVA ASDs. Que. et al. showed that the very high  $T_g$  compound, ledipasvir, had an LoC of less than 5% DL (12). Saboo et al. studied the release of indomethacin from ASDs as a function of temperature and found that the LoC was decreased upon lowering the temperature to below the estimated  $T_g$  of the water-saturated ASD (13). Likewise, Yang et al. found the LoC of loratadine-PVPVA ASDs decreased from 30% to <10% upon decreasing the temperature from 37°C to

5°C (84). CPD has a  $T_g$  of  $-9^\circ\text{C}$  and thus reduces the  $T_g$  of the resultant ASD (supplementary information, section S4). The increased polymer release rate in the presence of the low  $T_g$  drug is consistent with other studies that demonstrate that additives that change the  $T_g$  of the system can increase dissolution rate. Thus 20 wt.% of poly(ethylene oxide) (PEO) increased the dissolution rate of polymethyl methacrylate (PMMA) by a factor of two due to a plasticization effect where the  $T_g$  of the system was lowered (85).

The second factor favorable to the high LoC is the lack of specific interactions between the drug and polymer; neither CPD nor PVPVA have any hydrogen bond donors. It has also been found that drugs that form strong hydrogen bonds with PVPVA tend to have lower LoCs. For example, Saboo et al. compared the LoC for indomethacin (strong hydrogen bonding with polymer) versus the methyl ester (no hydrogen bonding) and found a much lower LoC for the former compound (13). Similar results were observed in a recent study, where all the compounds with good hydrogen bonding potential with the polymer were found to have low LoCs. However, given that these particular drugs also had high  $T_g$ 's it is somewhat difficult to deconvolute these two effects (84). The lack of interaction between CPD and PVPVA is further exemplified by centrifugation studies (supplementary information, section S4), where it was found that a minimal amount of PVPVA was present in the CPD nanoparticles (<5%). This is in contrast to a study with ibuprofen which is known to form strong interactions with PVPVA, where extensive PVPVA partitioning into the drug-rich nanodrops was observed (60).

While a low  $T_g$  of the formulation is emerging as a favorable factor for drug release, the higher mobility of such systems enables potentially undesirable phase transformations including crystallization and amorphous-amorphous phase separation (AAPS). While CPD free base does not undergo crystallization, the images shown in Fig. 11 suggest that there is a tendency for CPD-PVPVA ASDs to undergo water-induced AAPS. Solvent-induced phase separation occurs when one component has a much higher affinity for the solvent relative to the other component. Here, PVPVA has a much higher affinity for water than CPD, which is a lipophilic compound with a cLog P 3.8, and hence has unfavorable interactions with water (86). Formation of drug-rich domains reduces the extent of unfavorable drug-water interactions. Both the 50 and 60% DL binary ASDs show clear evidence of phase separation in ASD films, forming bicontinuous drug-rich and polymer-rich domains. In contrast, over a short time period, the 40% DL ASD remained homogeneous. Phase separation of

drug and polymer, in particular when sufficient drug-rich phase is present to be able to form a continuous or semi-continuous barrier layer at the surface of the dissolving ASD, is linked to a deterioration of release performance. Micro-CT imaging in combination with surface analysis have shown that higher DL PVPVA ASDs tend to show the formation of a porous, drug-rich layer at the ASD-water interface (12, 77, 81). For the CPD-PVPA ASDs, results also support a link between extensive phase separation at 50% DL and above and a deterioration in release performance for ASDs of the corresponding composition. Thus, at high DLs, AAPS is proposed to occur rapidly, with the formation of a continuous drug-rich phase (Fig. 11f), with subsequent rapid polymer dissolution, and surface enrichment of drug, leading to very low drug release.

### Impact of Surfactants on Release

Surfactants are commonly used in ASD formulation for various purposes including as solubilizers, and to improve the rheological properties during processing (29–31). Likewise, addition of surfactant has been found to facilitate release of the drug from the polymer-drug dispersion by improving surface wetting, contributing to faster dissolution (31, 87). Product labels reveal that several approved ASD products contain surfactants. Incivek®, Kalydeco®, Astagraf XL®, and Okambi® contain SDS, Zepatier® and Mavyret contain TPGS, while Venclexta® has Tween®80 in its formulation. It is not known, however, if the surfactant is part of the ASD intermediate, or externally added to the final formulation.

For various drugs, incorporation of surfactants into the ASD has been found to increase the LoC. Que. et al. increased the LoC of ledipasvir-PVPVA ASDs from 5% to 30% DL by adding SDS while in another study (12), TPGS was found to improve the release of felodipine from 10 to 35% DL, again in PVPVA ASDs (68). Likewise, Harmon et al. found that incorporation of TPGS in anacetrapib ASDs drastically improved drug release when the drug loading was 20% (20). Out of the surfactants evaluated herein, only SDS was found to favorably improve the release profile of CPD, extending the LoC from 40 to 50% DL. Incorporation of CTAB had a negative impact on the release profile, with the decline in the amount of drug released with time being attributed to agglomeration of the CPD-rich phase, as seen in the solution studies. Interestingly, the non-ionic surfactants, which appear to have more extensive interactions with CPD based on the NMR studies, reduced the rate of drug and polymer release, relative to the corresponding binary ASD, an effect that is

most noticeable for the TPGS-containing ASDs. This is likely unfavorable for an ASD formulation unless a slower release rate is desired. SDS appeared to be the best surfactant choice for CPD. In terms of a plausible mechanism for the improvements observed with SDS, we note from the confocal microscope images shown in Fig. 12, that the 50% DL ASD film remains homogeneous (within the detection limit of the measurement which is ~500 nm) when SDS is present, in contrast to the extensive phase separation observed in the absence of surfactant. Thus, SDS may prevent, delay, or change the domain size of phase separation at this drug loading, leading to improved release. The surfactant is not effective at preventing visible phase separation when the DL is increased to 60%, consistent with the poor release performance of this ASD. In contrast, TPGS and TWN clearly do not prevent phase separation, consistent with the lack of improvement in the release. TPGS in particular, appears to enhance the rate of ripening of the phase separated domains, which can possibly be explained by partitioning of this surfactant into the CPD-rich phase, as inferred from the NMR measurements, with a resultant change in the kinetics and thermodynamics of the system.

## CONCLUSIONS

ASDs of clopidogrel with PVPVA showed a high limit of congruency (LoC) relative to those reported for other PVPVA-based dispersions, where near-congruent and rapid release of drug and polymer was observed for drug loadings of 40%. Interestingly, the normalized release rate of PVPVA in the ASD with clopidogrel was increased relative to the release rate of neat polymer. This is somewhat counterintuitive given the lipophilicity of clopidogrel and the high drug loading. The high LoC was attributed to the low  $T_g$  of the drug and a lack of specific interactions with the polymer, and the increased polymer release rate is thought to result from a plasticization effect of the drug. Among the several surfactants tested, only SDS improved the release performance at high drug loading, increasing the LoC to 50% DL. Surfactants were found to interact differently with CPD, whereby non-ionic surfactants tended to partition into the drug-rich phase, while ionic surfactants interacted at the nanodroplet-water interface. Some of the surfactants showed benefits in terms of stabilizing the nanodroplet size, while somewhat surprisingly, CTAB destabilized the nanodroplets, with rapid size enlargement. Different kinetics and morphology of water-induced phase separation were observed depending on surfactants type present in the ASD, although

the significance of such differences to ASD release performance, if any, is currently unknown. These observations further our understanding of factors impacting drug release from ASDs, but also highlight the complexity of the release process. Finally, it is apparent that there are still many gaps in our understanding of ASD release performance that need to be addressed to effectively implement this solubility enhancing strategy for a broad swathe of APIs.

**ACKNOWLEDGMENTS AND DISCLOSURES** The authors would like to thank Abbvie Inc., for the financial support. The authors declare the following competing financial interest(s): Purdue University and AbbVie jointly participated in study design, research, data collection, analysis and interpretation of data, writing, reviewing, and approving the publication. C.C.S. is a graduate students; L.S.T. is a professor; all are at Purdue University. K.U. was a visiting scholar at Purdue University at the time of the study; They all have no additional conflicts of interest to report. A.S.I., Y.G., and G.G.Z.Z. are employees of AbbVie and may own AbbVie stock.

## REFERENCES

1. Amidon GL, Lennernäs H, Shah VP, Crison JR. A theoretical basis for a biopharmaceutical drug classification: the correlation of *in vitro* drug product dissolution and *in vivo* bioavailability. *Pharm Res: Off J Am Assoc Pharm Sci.* 1995;12:413–20.
2. Taylor LS, Zhang GGZ. Physical chemistry of supersaturated solutions and implications for oral absorption. *Adv Drug Deliv Rev.* 2016;101:122–42.
3. Indulkar AS, Gao Y, Raina SA, Zhang GGZ, Taylor LS. Exploiting the phenomenon of liquid-liquid phase separation for enhanced and sustained membrane transport of a poorly water-soluble drug. *Mol Pharm.* 2016;13:2059–69.
4. Lu J, *et al.* Impact of endogenous bile salts on the thermodynamics of supersaturated active pharmaceutical ingredient solutions. *Cryst Growth Des.* 2017;17:1264–75.
5. Indulkar AS, *et al.* Impact of micellar surfactant on supersaturation and insight into Solubilization mechanisms in supersaturated solutions of Atazanavir. *Pharm Res.* 2017;34:1276–95.
6. Coan KED, Shoichet BK. Stoichiometry and physical chemistry of promiscuous aggregate-based inhibitors. *J Am Chem Soc.* 2008;130:9606–12.
7. Ilevbare GA, Taylor LS. Liquid-liquid phase separation in highly supersaturated aqueous solutions of poorly water-soluble drugs: implications for solubility enhancing formulations. *Cryst Growth Des.* 2013. <https://doi.org/10.1021/cg301679h>.
8. Paus R, Ji Y, Vahle L, Sadowski G. Predicting the solubility advantage of amorphous pharmaceuticals: A novel thermodynamic approach. *Mol Pharm.* 2015;12:2823–33.

9. Mosquera-Giraldo LI, Taylor LS. Glass–liquid phase separation in highly supersaturated aqueous solutions of telaprevir. *Mol Pharm*. 2015;12:496–503.
10. Indulkar AS, Box KJ, Taylor R, Ruiz R, Taylor LS. pH-dependent liquid-liquid phase separation of highly supersaturated solutions of weakly basic drugs. *Mol Pharm*. 2015;12:2365–77.
11. Kesisoglou F, *et al*. Effect of amorphous nanoparticle size on bioavailability of Anacetrapib in dogs. *J Pharm Sci*. 2019;108:2917–25.
12. Que C, *et al*. Insights into the dissolution behavior of Ledipasvir-Copovidone amorphous solid dispersions: role of drug loading and intermolecular interactions. *Mol Pharm*. 2019;16:5054–67.
13. Saboo S, Kestur US, Flaherty DP, Taylor LS. Congruent release of drug and polymer from amorphous solid dispersions: insights into the role of drug-polymer hydrogen bonding, surface crystallization, and glass transition. *Mol Pharm*. 2020;17:1261–75.
14. Ganesh AN, Donders EN, Shoichet BK, Shoichet MS. Colloidal aggregation: from screening nuisance to formulation nuance. *Nano Today*. 2018;19:188–200.
15. Raina SA, *et al*. Impact of solubilizing additives on supersaturation and membrane transport of drugs. *Pharm Res*. 2015;32:3350–64.
16. Indulkar AS, Lou X, Zhang GGZ, Taylor LS. Insights into the dissolution mechanism of ritonavir-Copovidone amorphous solid dispersions: importance of congruent release for enhanced performance. *Mol Pharm*. 2019;16:1327–39.
17. Auch C, Jede C, Harms M, Wagner C, Mäder K. Impact of amorphization and GI physiology on supersaturation and precipitation of poorly soluble weakly basic drugs using a small-scale *in vitro* transfer model. *Int J Pharm*. 2020. <https://doi.org/10.1016/j.ijpharm.2019.118917>.
18. Dressman JB, Reppas C. *In vitro-in vivo* correlations for lipophilic, poorly water-soluble drugs. *Eur J Pharm Sci*. 2000. [https://doi.org/10.1016/S0928-0987\(00\)00181-0](https://doi.org/10.1016/S0928-0987(00)00181-0).
19. Wilson V, *et al*. Relationship between amorphous solid dispersion *in vivo* absorption and *in vitro* dissolution: phase behavior during dissolution, speciation, and membrane mass transport. *J Control Release*. 2018;292:172–82.
20. Harmon P, *et al*. Mechanism of dissolution-induced nanoparticle formation from a Copovidone-based amorphous solid dispersion. *Mol Pharm*. 2016;13:1467–81.
21. Stewart AM, *et al*. Impact of Drug-Rich Colloids of Itraconazole and HPMCAS on Membrane Flux *in Vitro* and Oral Bioavailability in Rats. *Mol Pharm*. 2017. <https://doi.org/10.1021/acs.molpharmaceut.7b00338>.
22. Sugano K. Possible reduction of effective thickness of intestinal unstirred water layer by particle drifting effect. *Int J Pharm*. 2010. <https://doi.org/10.1016/j.ijpharm.2009.12.014>.
23. Ilevbare GA, Liu H, Pereira J, Edgar KJ, Taylor LS. Influence of additives on the properties of nanodroplets formed in highly supersaturated aqueous solutions of ritonavir. *Mol Pharm*. 2013;10:3392–403.
24. Lindfors L, *et al*. Amorphous drug nanosuspensions. 2. Experimental determination of bulk monomer concentrations. *Langmuir*. 2006;22:911–6.
25. Ueda K, Yamamoto N, Higashi K, Moribe K. Molecular mobility suppression of ibuprofen-rich amorphous Nanodroplets by HPMC revealed by NMR Relaxometry and its significance with respect to crystallization inhibition. *Mol Pharm*. 2019. <https://doi.org/10.1021/acs.molpharmaceut.9b00840>.
26. Urbina-villalba G, Cruz-Barrios E. Influence of creaming and ripening on the aggregation rate of non-ionic Dodecane-in-water Nanoemulsions. *Rev del CEIF*. 2014;3:22–9.
27. Sun Y, Deac A, Zhang GGZ. Assessing physical stability of colloidal dispersions using a Turbiscan optical analyzer. *Mol Pharm*. 2019;16:877–85.
28. Tadros TF. *Applied surfactants: principles and applications*: Wiley-VCH Verlag GmbH & Co; 2006.
29. Chen J, Ormes JD, Higgins JD, Taylor LS. Impact of surfactants on the crystallization of aqueous suspensions of celecoxib amorphous solid dispersion spray dried particles. *Mol Pharm*. 2015;12:533–41.
30. Jermain SV, Brough C, Williams RO. Amorphous solid dispersions and nanocrystal technologies for poorly water-soluble drug delivery – an update. *Int J Pharm*. 2018;535:379–92.
31. Solanki NG, *et al*. Effects of surfactants on Itraconazole-HPMCAS solid dispersion prepared by hot melt extrusion. I: miscibility and drug release. *J Pharm Sci*. 2018;1–13. <https://doi.org/10.1016/j.xphs.2018.10.058>.
32. Tadros TF. 2. Interfacial aspects of pharmaceutical systems. *Interfacial Phenom Colloid Stab*. 2015. <https://doi.org/10.1515/9783110366471-004>.
33. Merisko-Liversidge E, Liversidge GG, Cooper ER. Nanosizing: A formulation approach for poorly-water-soluble compounds. *Eur J Pharm Sci*. 2003;18:113–20.
34. Gershanik T, Benita S. Self-dispersing lipid formulations for improving oral absorption of lipophilic drugs. *Eur J Pharm Biopharm*. 2000;50:179–88.
35. Chavda VP, Shah D. Self-emulsifying delivery systems: One step ahead in improving solubility of poorly soluble drugs. *Nanostructures for Cancer Therapy*: Elsevier Inc; 2017. <https://doi.org/10.1016/B978-0-323-46144-3.00025-8>.
36. Mosquera-Giraldo LI, Trasi NS, Taylor LS. Impact of surfactants on the crystal growth of amorphous celecoxib. *Int J Pharm*. 2014;461:251–7.
37. Indulkar AS, Gao Y, Raina SA, Zhang GGZ, Taylor LS. Impact of monomeric *versus* micellar surfactant and surfactant-polymer interactions on nucleation-induction times of Atazanavir from supersaturated solutions. *Cryst Growth Des*. 2020;20:62–72.
38. Ananthapadmanabhan KP, Goddard ED, Turro NJ, Kuo PL. Fluorescence probes for critical micelle concentration. *Langmuir*. 1985;1:352–5.
39. Bhattacharjee S. DLS and zeta potential - what they are and what they are not? *J Control Release*. 2016;235:337–51.
40. Claridge TDW. High-resolution NMR techniques in organic chemistry. Chapter 12: Elsevier; 2016. <https://doi.org/10.1016/B978-0-08-099986-9/00012-9>.
41. RStudio Team. Rstudio: integrated development environment for R. (2020).
42. Purohit HS, Taylor LS. Phase behavior of ritonavir amorphous solid dispersions during hydration and dissolution. *Pharm Res*. 2017;34:2842–61.
43. Purohit HS, *et al*. Insights into Nano- and Micron-scale phase separation in amorphous solid dispersions using fluorescence-based techniques in combination with solid state nuclear magnetic resonance spectroscopy. *Pharm Res*. 2017;34:1364–77.
44. Wang L, Gaigalas AK, Reipa V. Optical properties of Alexa<sup>TM</sup> 488 and cy<sup>TM</sup>5 immobilized on a glass surface. *Biotechniques*. 2005;38:127–31.
45. ICI Americas Inc. The HLB System. A time-saving Guid Emuls Sel. 1980;37:1390–3.
46. Miraglia DB, Rodríguez JL, Minardi RM, Schulz PC. Critical micelle concentration and HLB of the sodium

- oleate- hexadecyltrimethylammonium bromide mixed system. *J Surfactant Deterg.* 2011;14:401–8.
47. Zhang Z, Tan S, Feng SS. Vitamin E TPGS as a molecular biomaterial for drug delivery. *Biomaterials.* 2012;33:4889–906.
48. Fuguet E, Rafols C, Rosés M, Bosch E. Critical micelle concentration of surfactants in aqueous buffered and unbuffered systems. *Anal Chim Acta.* 2005;95–100. <https://doi.org/10.1016/j.aca.2005.05.069>.
49. Chauhan S, Chauhan MS, Kaushal D, Syal VK, Jyoti J. Study of micellar behavior of SDS and CTAB in aqueous media containing furosemide-A cardiovascular drug. *J Solut Chem.* 2010;39:622–38.
50. Mahmood M, Al-koofee D. Effect of temperature changes on critical micelle concentration for tween series surfactant. *Glob J Sci Front Res Chem.* 2013;13:1–7.
51. Patist A, Bhagwat SS, Penfield KW, Aikens P, Shah DO. On the measurement of critical micelle concentrations of pure and technical-grade nonionic surfactants. *J Surfactant Deterg.* 2000;3:53–8.
52. Wan LSC, Lee PFS. CMC of polysorbates. *J Pharm Sci.* 1974;63:136–7.
53. Croy SR, Kwon GS. Polysorbate 80 and Cremophor EL micelles Deaggregate and solubilize nystatin at the Core – Corona Interface. *J Pharm Sci.* 2005;94:2345–54.
54. Tang X, Huston KJ, Larson RG. Molecular dynamics simulations of structure-property relationships of tween 80 surfactants in water and at interfaces. *J Phys Chem B.* 2014;118:12907–18.
55. Amani A, York P, De Waard H, Anwar J. Molecular dynamics simulation of a polysorbate 80 micelle in water. *Soft Matter.* 2011;7:2900–8.
56. Sadoqi M, Lau-cam CA, Wu SH. Investigation of the micellar properties of the tocopheryl polyethylene glycol succinate surfactants TPGS 400 and TPGS 1000 by steady state fluorometry. *J Colloid Interface Sci.* 2009;333:585–9.
57. Pant D, Levinger NE. Polar solvation dynamics of H<sub>2</sub>O and D<sub>2</sub>O at the surface of zirconia nanoparticles. *J Phys Chem B.* 1999;103:7846–52.
58. Claridge TDW. High-resolution NMR techniques in organic chemistry. Chapter 2: Elsevier; 2016. <https://doi.org/10.1016/B978-0-08-099986-9/00002-6>.
59. Apperley DC, *et al.* Characterisation of indomethacin and nifedipine using variable-temperature solid-state NMR. *Magn Reson Chem.* 2005;43:881–92.
60. Ueda K, Taylor LS. Polymer type impacts amorphous solubility and drug-rich phase colloidal stability: A mechanistic study using nuclear magnetic resonance spectroscopy. *Mol Pharm.* 2020. <https://doi.org/10.1021/acs.molpharmaceut.0c00061>.
61. Ueda K, Higashi K, Moribe K. Direct NMR monitoring of phase separation behavior of highly supersaturated Nifedipine solution stabilized with Hypromellose derivatives. *Mol Pharm.* 2017;14:2314–22.
62. Ueda K, Taylor LS. Partitioning of surfactant into drug-rich nanodroplets and its impact on drug thermodynamic activity and droplet size. *J Control Release.* 2021;330:229–43.
63. Aguiar J, Carpena P, Molina-Bolivar JA, Carnero Ruiz C. On the determination of the critical micelle concentration by the pyrene 1:3 ratio method. *J Colloid Interface Sci.* 2003;258:116–22.
64. Williams RJ, Phillips JN, Mysels KJ. The critical micelle concentration of sodium lauryl sulphate at 25° C. *Trans Faraday Soc.* 1955;51:728–37.
65. Furihata K, Zhang J, Koda M, Miyakawa T, Tanokura M. Broadband WET: A novel technique for quantitative characterization of minor components in foods. *Magn Reson Chem.* 2014;52:333–8.
66. Adams RW, Holroyd CM, Aguilar JA, Nilsson M, Morris GA. “Perfecting” WATERGATE: clean proton NMR spectra from aqueous solution. *Chem Commun.* 2013;49:358–60.
67. Maiwald M, Steinhof O, Sleigh C, Bernstein M, Hasse H. Quantitative high-resolution online NMR spectroscopy in pharmaceutical reaction and process monitoring. *NMR Spectrosc Pharm Anal.* 2008;471–91. <https://doi.org/10.1016/B978-0-444-53173-5.00020-2>.
68. Saboo S, Bapat P, Moseson DE, Kestur US, Taylor LS. Exploring the role of surfactants in enhancing drug release from amorphous solid dispersions at higher drug loadings. *Pharmaceutics.* 2021;13:1–22.
69. Han YR, Ma Y, Lee PI. Impact of phase separation morphology on release mechanism of amorphous solid dispersions. *Eur J Pharm Sci.* 2019;136:104955.
70. Greenspan P, Fowler SD. Spectrofluorometric studies of the lipid probe, Nile red. *J Lipid Res.* 1985;26:781–9.
71. Sackett DL, Wolff J. Nile red as a polarity-sensitive fluorescent probe of hydrophobic protein surfaces. *Anal Biochem.* 1987;167:228–34.
72. Zanetti-Domingues LC, Tynan CJ, Rolfe DJ, Clarke DT, Martin-Fernandez M. Hydrophobic fluorescent probes introduce artifacts into single molecule tracking experiments due to non-specific binding. *PLoS One.* 2013;8.
73. Thermo Fisher. Thermo Fisher Scientific. <https://www.thermo.com/us/en/home/brands/molecular-probes/key-molecular-probes-products/alexa-fluor/alexa-fluor-frequently-asked-questions.html#chem>. Accessed 9 July 2021.
74. De Aguiar HB, Strader ML, De Beer AGF, Roke S. Surface structure of sodium dodecyl sulfate surfactant and oil at the oil-in-water droplet liquid/liquid interface: A manifestation of a nonequilibrium surface state. *J Phys Chem B.* 2011;115:2970–8.
75. Stache H. Anionic surfactants: organic chemistry: Marcel Dekker; 1996.
76. Magee RW. Evaluation of the external surface area of carbon black by nitrogen adsorption. *Rubber Chem Technol.* 1994;68:11–4.
77. Saboo S, Moseson DE, Kestur US, Taylor LS. Patterns of drug release as a function of drug loading from amorphous solid dispersions: A comparison of five different polymers. *Eur J Pharm Sci.* 2020;155:105514.
78. Chen Y, *et al.* Drug-polymer-water interaction and its implication for the dissolution performance of amorphous solid dispersions. *Mol Pharm.* 2015;12:576–89.
79. Mosquera-Giraldo LI, *et al.* Influence of polymer and drug loading on the release profile and membrane transport of telaprevir. *Mol Pharm.* 2018. <https://doi.org/10.1021/acs.molpharmaceut.8b00104>.
80. Indulkar AS, *et al.* Origin of Nanodroplet formation upon dissolution of an amorphous solid dispersion: A mechanistic isotope scrambling study. *J Pharm Sci.* 2017;106:1998–2008.
81. Saboo S, Mugheirbi NA, Zemlyanov DY, Kestur US, Taylor LS. Congruent release of drug and polymer: A “sweet spot” in the dissolution of amorphous solid dispersions. *J Control Release.* 2019;298:68–82.
82. Papanu JS, Soane SDS, Bell AT, Hess DW. Transport models for swelling and dissolution of thin polymer films. *J Appl Polym Sci.* 1989;38:859–85.
83. Ouano AC, Carothers JA. Dissolution dynamics of some polymers: solvent-polymer boundaries. *Polym Eng Sci.* 1980;20:160–6.
84. Yang R, *et al.* Drug release and Nanodroplet formation from amorphous solid dispersions: insight into the roles of drug

- physicochemical properties and polymer selection. *Mol Pharm.* 2021. <https://doi.org/10.1021/acs.molpharmaceut.1c00055>.
85. Cooper WJ, Krasicky PD, Rodriguez F. Effects of molecular weight and plasticization on dissolution rates of thin polymer films. *Polymer (Guildf)*. 1985;26:1069–72.
86. (2020), N. C. for B. I. PubChem Compound Summary for CID 60606, Clopidogrel. Retrieved November 19, 2020. <https://pubchem.ncbi.nlm.nih.gov/compound/Clopidogrel>. Accessed 19 Nov 2020.
87. Qi S, *et al.* Insights into the role of polymer-surfactant complexes in drug solubilisation/stabilisation during drug release from solid dispersions. *Pharm Res.* 2013;30:290–302.

**Publisher's Note** Springer Nature remains neutral with regard to jurisdictional claims in published maps and institutional affiliations.